89 P

Frequency Domain Analysis of the Random Loading of Cracked Panels

By

James F. Doyle, Principal Investigator
SCHOOL OF AERONAUTICS AND ASTRONAUTICS
PURDUE UNIVERSITY
WEST LAFAYETTE, INDIANA 47907

Final Report:
For the period October 1, 1990 to September 30, 1993

Prepared for:
NASA LANGLEY RESEARCH CENTER
HAMPTON, VA 23681-0001

Under:
NASA RESEARCH GRANT NAG 1-1173
DR. STEPHEN A. RIZZI, TECHNICAL MONITOR
STRUCTURAL ACOUSTICS BRANCH, ACOUSTICS DIV.

June 16, 1994

Foreword

This report summarizes the research accomplishments performed under the NASA langley Research Center Grant No. NAG 1-1173, entitled: "Frequency Domain Analysis of the Random Loading of Cracked Panels," for the period October 1, 1990 to September 30, 1993. The primary effort of this research project was focused on the development of analytical methods for the accurate prediction of the effect of random loading on a panel with a crack. Of particular concern was the influence of frequency on the stress intensity factor behavior.

Contents

INTRODUCTION

Many modern structures, such as those found in advanced aircraft, are lightweight and consequently dynamic response plays a very important role in their analysis. The analysis of vibration response is of considerable importance in the design of structures that may be subjected to dynamic disturbances. Under certain situations, vibrations may cause large displacements and severe stresses in the structure. This may happen when the frequency of the exciting force spans a natural frequency of the structure and *resonance* ensues. A related problem is that fluctuating stresses, even of moderate intensity, may cause material failure through fatigue and wear. Also, the transmission of vibrations to connected structures may lead to undesirable consequences: delicate instruments may malfunction or human occupants may suffer discomfort.

With the increasing use being made of lightweight, high-strength materials, structures today are more susceptible than ever before to critical vibrations. Modern buildings and bridges are lighter, more flexible, and are made of materials that provide much lower energy dissipation; all of these contribute to more intense vibration responses. Dynamic analysis of structures is therefore important for modern structures, and likely to become even more so.

The presence of flaws and cracks in a material or structure can have catastrophic consequences. To be able to analyze these situations is the main reason for concepts of fracture mechanics. It is well known that, in addition to the material properties, the fatigue life of a structural component is influenced by the amplitude, sequence and frequency of the applied stresses as well as environmental effects. In the design of critical structures such as those used in automobiles and aircraft, for example, it is essential to consider these factors and to include fatigue in the analysis in order to guarantee their safety and reliability [22].

The stress intensity factor, K, emerges as a very significant parameter that characterizes the crack behavior. Even though the stress at the crack tip tends to infinity for all cracks, K can be used to distinguish between the severity of the loading in different crack situations.

We are interested in analyzing the dynamic response of panels that contain cracks. We will use the finite element method but because this type of problem is inherently computationally intensive we explore a number of ways of doing this more efficiently. One method to find K is to use its definition as a limit toward the crack tip. A very fine mesh must be used in order to model the severe geometry change and a fine mesh must also be used remotely so as to model the dynamic characteristics of the plate. This method of calculating K was used in Reference [15] as a baseline method. This method is too computationally expensive to be used for the present problems. Alternative methods of calculating K in an efficient manner are addressed; three alternative methods are the focus of this research. Each of the three methods uses classical plate theory in performing the analysis.

Outline of Report

We begin, in Section 1, by reviewing the finite element method and establishing its baseline performance. The discrete Kirchhoff triangle (DKT) element is used and we show its convergence behavior for some static and dynamic problems.

Section 2 introduces the virtual crack closure technique for static stress intensity calculation. This method is based on a work-energy type of relation. It has the significant advantage that the local singularity, as represented by K, can be obtained from work done by the crack forces. For the opening mode, for example,

$$K = \sqrt{\frac{3E(3+\nu)G}{(1+\nu)h}}, \qquad G = \frac{M_x \Delta\phi_x}{2\Delta a}$$

where G is the strain energy release rate, M_x is a moment exerted on the crack tip, and $\Delta\phi_x$ is the opening rotation of the nodes closest to the crack tip. The performance of this method is checked against available handbook solutions.

The frequency domain view of crack dynamics is developed in Section 3. First, by defining a frequency domain concept of work, we extend the virtual crack closure

method to situations involving damping. It is shown that the crack response and structural response are very similar in character—actually the crack response is dominated by the structural response. This leads to a global response spectrum method summarized by

$$\hat{K}(\omega) = K_s \frac{\hat{\phi}(\omega)}{\phi_o(0)}$$

where $\hat{\phi}(\omega)$ is the rotation obtained by a modal analysis, ϕ_o is its static value, and K_s is the static stress intensity obtained either by analysis or from a handbook. The essence of this equation is that a 'crack analysis' need only be done for the static case.

Section 4 considers the time responses due to transient loading. There are two methods investigated: time integrations, and frequency domain convolution represented by

$$u(t) = \sum \hat{u} e^{iwt} = \sum \hat{H} \hat{P} e^{iwt}$$

where $\hat{H}(w)$ is the frequency response function. Each method further divides into direct use of finite elements or indirectly using modal analysis. The inverse FFT is taken of the frequency domain quantities in order to find them in the time domain.

The final section considers a very computationally intensive problem—random dynamic loading of a panel with a crack. Based on the conclusions of Section 4 only the modal based methods are applied here.

A common thread running through this research is the notion that the dynamics of cracked panels divides into separate effects of global dynamic behavior of the panel and local crack tip singularity. In other words, we see an almost static crack embedded in a structure (sans singularity) which is behaving dynamically. This frees us to bring to bear the most effective tools for each separate area.

1. FINITE ELEMENT MODELING

This section reviews the formulation of the finite element modeling and performs some baseline tests for judging its accuracy. The information gained here will be used to decide on the model to be used in the later studies. Testing involved different mesh sizes, boundary conditions, and loadings; whenever possible, the results from the finite element analysis are compared to the available analytical results. The purpose of this section is to also exercise the program PlaDyn [13] over the range of problems to be considered later.

1.1 Discrete Kirchhoff Triangular Element

We consider only thin plate theory (Kirchhoff plates) and the element used to model this behavior is the discrete Kirchhoff triangle element (DKT). Kirchhoff plate theory is applied here in that the transverse shear deformation is assumed to be zero; versus Mindlin plate theory, which assumes transverse shear deformation is allowed. Therefore, Mindlin plate theory is especially suited to thick plates and sandwich plates [3].

This element has a node at each corner of the triangle with degrees of freedom $\{w, \phi_x, \phi_y\}$ at each node. In local coordinates it has a total of 9 degrees of freedom. In the derivation of the element, the deflection and rotations are assumed to have the representations (similar to Mindlin plate theory)

$$w = \sum_i^6 N_i w_i\,, \qquad \phi_x = \sum_i^6 N_i \phi_{xi}\,, \qquad \phi_y = \sum_i^6 N_i \phi_{yi} \tag{1.1}$$

where $N_i = (2L_i - 1)L_i$ for i=1, 2, 3, $N_4 = 4L_1L_2$, $N_5 = 4L_2L_3$ and $N_6 = 4L_3L_1$. The parameters L_i are areal coordinates and are shown in Figure 1.1. These parameters can be expressed as

$$L_i = \frac{1}{2A}(A_i^o + a_i x + b_i y) \qquad i = 1,2,3 \tag{1.2}$$

where A_i^o, a_i, and b_i are given as

$$A_i^o = x_j y_l - x_l y_j \tag{1.3}$$

$$a_i = y_j - y_l \tag{1.4}$$

$$b_i = x_l - x_j \tag{1.5}$$

where (x_i, y_i) are the coordinates of the node i (i=1, 2, 3) [12]. In this, there are a total of 18 unknowns. Hence, initially there are more degrees of freedom than will appear in the final form of the element. The extra degrees of freedom are eliminated as follows. The in-plane strains (ϵ_x, ϵ_y, and γ_{xy}) are evaluated from the strain-displacement relations of Mindlin plate theory; consequently, element strains and strain energy depend on ϕ_x and ϕ_y but are independent of w. Next, with the shear strains $\gamma_{zy} = \gamma_{zx} = 0$ in the Mindlin plate equations, we impose Kirchhoff constraints of $\partial w/\partial y - \phi_y$=0 and $\partial w/\partial x - \phi_x$=0 at certain points. These particular points are taken at points midway along the sides, and are sufficient in number to eliminate the extra degrees of freedom. This leads to the coupling of the rotations with the deflection. This element was first introduced by Stricklin, Haisler, Tisdale, and Gunderson in 1968 [20]. The derivation of the element is based on requiring the transverse shear deformation to be zero at the nodes and along the sides of the element and proceeds as follows.

Consider a laminate of thickness dz located a distance z from the midsurface of the plate as shown in Figure 1.2. The displacements of this laminate are represented by

$$\begin{aligned} u = z\Big[&L_1(2L_1-1)\frac{\partial u_1}{\partial z} + L_2(2L_2-1)\frac{\partial u_2}{\partial z} \\ &+L_3(2L_2-1)\frac{\partial u_3}{\partial z} 4L_1L_2\frac{\partial u_4}{\partial z} + 4L_2L_3\frac{\partial u_5}{\partial z} + 4L_1L_3\frac{\partial u_6}{\partial z}\Big] \end{aligned} \tag{1.6}$$

$$\begin{aligned} v = z\Big[&L_1(2L_1-1)\frac{\partial v_1}{\partial z} + L_2(2L_2-1)\frac{\partial v_2}{\partial z} \\ &+L_3(2L_2-1)\frac{\partial v_3}{\partial z} 4L_1L_2\frac{\partial v_4}{\partial z} + 4L_2L_3\frac{\partial v_5}{\partial z} + 4L_1L_3\frac{\partial v_6}{\partial z}\Big] \end{aligned} \tag{1.7}$$

$$w = L_1^2(L_1 + 3L_2 + 3L_3)w_1 + L_1^2(c_3L_2 - c_2L_3)\frac{\partial w_1}{\partial x} \qquad (1.8)$$
$$+L_1^2(b_2L_3 - b_3L_2)\frac{\partial w_1}{\partial y} + ... + \alpha L_1L_2L_3$$

where u, v, w are displacements in x, y, and z directions, respectively; L_1, L_2, L_3 are area coordinates; $b_i = y_j - y_k$; $c_i = x_k - x_j$; and α is a generalized coefficient. The additional six terms for w are obtained by cyclic permutation.

A nine degree of freedom element is obtained both by requiring the transverse shear strains to be zero at the corners and along the sides of the element and by assuming the slope normal to the element at the middle of the side is one half the sum of the values at the corner nodes. These conditions yield

$$\frac{\partial w_i}{\partial x} = -\frac{\partial u_i}{\partial z}; \qquad \frac{\partial w_i}{\partial y} = -\frac{\partial v_i}{\partial z}; \qquad i = 1,2,3 \qquad (1.9)$$

$$\frac{\partial u_4}{\partial z} = \frac{1}{b_3^2 + c_3^2}\left[\frac{3}{2}c_3w_1 + \left(\frac{b_3^2}{2} - \frac{c_3^2}{4}\right)\frac{\partial u_1}{\partial z} + \frac{3b_3c_3}{4}\frac{\partial v_1}{\partial z}\right. \qquad (1.10)$$
$$\left. -\frac{3}{2}c_3w_2 + \left(\frac{b_3^2}{2} - \frac{c_3^2}{4}\right)\frac{\partial u_2}{\partial z} + \frac{3b_3c_3}{4}\frac{\partial v_2}{\partial z}\right]$$

$$\frac{\partial v_4}{\partial z} = \frac{1}{b_3^2 + c_3^2}\left[-\frac{3}{2}b_3w_1 + \frac{3}{4}b_3c_3\frac{\partial u_1}{\partial z} + \left(\frac{c_3^2}{2} - \frac{b_3^2}{4}\right)\frac{\partial v_1}{\partial z}\right. \qquad (1.11)$$
$$\left. +\frac{3}{2}b_3w_2 + \frac{3}{4}b_3c_3\frac{\partial u_2}{\partial z} + \left(\frac{c_3^2}{2} - \frac{b_3^2}{4}\right)\frac{\partial v_2}{\partial z}\right]$$

The equations for $\partial u_5/\partial z$, $\partial v_5/\partial z$, $\partial u_6/\partial z$, $\partial u_6/\partial z$ are obtained by cyclic permutation. Interelement compatibility is still satisfied after Eqns. 1.9 through 1.11 are applied.

Neglecting the strain energy due to transverse shear, the strain energy expression for the element is the same as that used in plane-stress problems;

$$U = \frac{E}{1-\nu^2}\frac{1}{2}\int\left(\epsilon_x^2 + \epsilon_y^2 + 2\nu\epsilon_x\epsilon_y + \frac{1-\nu}{2}\epsilon_{xy}^2\right)dAdz \qquad (1.12)$$

where E is Young's modulus, ν is Poissons ratio, and the strains are $\epsilon_x = \partial u/\partial x$, $\epsilon_y = \partial v/\partial x$, $\epsilon_{xy} = \partial u/\partial y + \partial v/\partial x$.

It is noted that w does not enter the strain energy expression but enters through Eqns. 1.9 through 1.11. The element stiffness matrix is obtained by substituting the

assumed displacement functions into the strain energy expression and integrating over the volume of the element using the relation

$$\int L_1^i L_2^j L_3^k dA = [i!j!k!/(n+2)!]2A \tag{1.13}$$

where $n = i + j + k$ and A is the area of the element. The element stiffness matrix is symmetric and positive definite [20].

This DKT element has been widely researched and it has been documented that it is one of the more efficient elements for thin plate bending. Batoz, Bathe, and Ho [2] performed extensive testing on three different elements including the hybrid stress model (HSM), DKT element, and a selective reduced integration (SRI) element. Comparisons between the different element types were made based on the results from different mesh orientations and different boundary and loading conditions. The authors concluded that the DKT and HSM elements are the most effective elements available for bending analysis of thin plates. Of these two elements the DKT element was deemed superior to the HSM element based on the comparison between the experimental and theoretical results [2].

A significant advantage of triangular elements is that they can be conveniently mapped to form irregular shapes. Our mesh generator uses them to form a basic building block called a module. A module is a quadrilateral divided into four triangles (elements) by its diagonals as shown in Figure 1.3. In this way, we effectively have an arbitrary quadrilateral element with an additional node in the center. This element is implemented in the finite element package PlaDyn which was used for the analyses. This program is capable of performing static and dynamic analysis of folded flat plates; and it can analyze situations involving applied transient load history, forced frequency loading, stability analysis, and modal analysis [13].

1.2 Static Analysis

In performing the static analysis, two different boundary conditions for four different mesh sizes were considered. The two types of boundary conditions are all edges simply supported (S-S-S-S), and all edges clamped (C-C-C-C). Two loading conditions were also considered: one was such that a point load was applied at the center

of the plate, and the other was that of a uniformly distributed load. The meshes were constructed by using the mesh generating program GenMesh that is part of the PlaDyn package and a typical mesh is shown in Figure 1.4 . Four different module sizes were constructed using 2, 1, 0.5 and 0.33 inch (50.8, 25.4, 12.7, and 8.382 mm) square modules. The plate was 20 inches by 20 inches (508 mm), and the half-plate used was composed of 200, 800, 3200, and 7200 elements for the respective module sizes given. In constructing these meshes, symmetry about the y-axis of the panel was imposed in order to reduce the size of the matrices. From a vibrational point of view this means that half of the modes will be missing, however, it is deemed that the number of remaining modes are sufficient to allow adequate testing of the program and methods. In order to impose the symmetry condition, degrees of freedom were specified to be $u=\phi_y=0$ along the mid-plane line of symmetry.

Point Load

For the S-S-S-S case under point loading the solution for the deflection was derived in Reference [21]. This particular solution for an applied point load was obtained using Navier's solution method in double-series form. This double-series converges very rapidly and the first few terms give the deflection with great accuracy.

For a square plate with a point load applied at the center, the final expression for the deflection is given by

$$w_o = \frac{0.0116Pa^2}{D} \tag{1.14}$$

where a is the plate width, P is the applied point load, and D is the flexural rigidity of the plate given by

$$D = \frac{Eh^3}{12(1-\nu^2)} \tag{1.15}$$

In the examples to be discussed, Young's modulus, E, is 10 msi (69 GPa), Poissons ratio, ν, is 0.3 (since this is the value of ν that is used in Reference [21]), and plate thickness, h, is 0.1 inch (2.54 mm). The results are shown in Figure 1.5. What is encouraging is that even the relatively large module gives very good results.

In deriving the solution for the clamped case, the simply supported solution was used and superposed on this were the deflections due to moments distributed along

the edges. These moments were adjusted in such a manner as to satisfy the condition of zero slope along the edges. For a square plate where the point load is applied at the center, the series converges to

$$w_o = \frac{0.00560Pa^2}{D} \tag{1.16}$$

Figure 1.5 shows a comparison of the results. For a given mesh size, the deviation in this case is greater than for the simply supported case. However, as the module size gets smaller, there is a very nice convergence. Thus, even a module size of 0.5 (Δ/a=0.05) gives results better than 0.5%.

Distributed Load

In implementing the distributed load for the DKT element, by necessity, different shape functions must be used for calculating the equivalent load vector than is used for calculating the stiffness matrix. Through using areal coordinates for the triangle, we have

$$\{P\} = \int [N]\{q\}da \tag{1.17}$$

PlaDyn forms this equivalent load vector on an element by element basis [13].

For the S-S-S-S case under uniform loading, the solution was derived in Reference [21]. In particular for a square plate, the solution is derived in terms of a series and converges rapidly to give the deflection at the center as

$$w_o = \frac{0.00406q_oa^4}{D} \tag{1.18}$$

where q_o is the magnitude of the uniformly distributed load. The results are shown in Figure 1.6 and show excellent agreement especially for the smaller module size.

The second set of boundary conditions applied was all edges clamped. Again, the deflection is derived in terms of a series. For a square plate the series converges to

$$w_o = \frac{0.00126q_oa^4}{D} \tag{1.19}$$

The results are shown in Figure 1.6. Again, the finite element results show a very nice convergence. An explanation for the slight difference may be sought in the nature of

the clamped boundary condition. Most triangles along the boundary have six of the nine degrees of freedom set to zero, further, twelve of the eighteen degrees of freedom at a corner (formed by two elements) are set to zero. These conditions are probably over constraining the finite element solution.

1.3 Vibration Analysis

In performing dynamic problems a choice must be made concerning the method of assembling the mass matrix. Just as for the distributed load, we cannot give a mass formulation that is consistent with the DKT element. However, we do have two alternative formulations; the lumped and consistent mass formulations.

In the lumped mass formulation the total mass, given by ρAh, of the element is equally distributed, or lumped, at each node. No rotational inertias are assumed at the nodes. The consistent mass matrix formulation is assembled by using displacement functions that are based on areal coordinates and given by

$$[m] = \int \rho [N]^T [N] dV \tag{1.20}$$

Once the stiffness and mass matrices are assembled, PlaDyn uses the subspace iteration scheme to solve the eigenvalue problem. In this analysis a reduced eigensystem is established by iteration on a set of Ritz vectors. The advantage in using subspace iteration (over vector iteration, say) is that the convergence of the subspace and not of individual iteration vectors is achieved. Consequently, it is less likely to miss any eigenvectors during the search [11].

The resonant frequencies obtained using the consistent mass formulation were compared with resonant frequencies obtained using the lumped mass formulation. This comparison was made so as to determine if using a lumped mass matrix would yields adequate results. This was of interest since using a lumped mass formulation versus a consistent mass formulation gives a mass matrix that assembles much quicker, uses less disk space and also makes the analysis proceed more rapidly

The first boundary condition examined is the S-S-S-S case. Reference [10] gives

the following equation for the analytical frequency value:

$$\omega_{mn} = \sqrt{\frac{D}{\rho h}}\left[\left(\frac{m\pi}{a}\right)^2 + \left(\frac{n\pi}{b}\right)^2\right] \tag{1.21}$$

where a and b are the half-widths of the rectangular plate, m and n are the mode numbers. The results are shown in Figures 1.7 through 1.10. In each case, there is a very nice convergence to the exact solution as the module size decreases. For each case, convergence is from below indicating that the stiffness is underestimated or the mass is overestimated.

There is no closed form solution for the vibration of a clamped plate but the results from Reference [6] can be represented for a square plate in the form

$$\omega_{mn} = \frac{\lambda_{mn}}{a^2}\sqrt{\frac{D}{\rho h}} \tag{1.22}$$

The values of λ depend upon the mode. For example, the lowest mode, where m=n=1, has a value for λ of 36.0, giving a value for ω_{11} of 544.7 rads/s. Values for other modes and the associated λ values are given in the following table

m,n	λ
1,1	36.0
1,2	73.4
1,3	131.6
2,3	164.4
4,1	210.4
2,3	219.3

The comparisons for the consistent mass formulation are shown in Figures 1.9 and 1.10. Again, there is nice convergence to the referenced results for most modes. But there are two things to note. The larger module results show more deviation than the simply supported results. Also, while convergence is achieved from below, some of the converged results are overestimates. The reason for this is not clear.

The performance of the lumped mass matrix is shown in Figures 1.11 and 1.12, for the fifteenth mode. These plots clearly show that the two mass models converge to each other as the module size decreases. In light of these results, the indication is that using the lumped mass formulation would yield results almost as accurate

as the consistent mass formulation. What they also show us, however, is that (for the simply supported case) when the mesh is marginal (i.e., large module size) the consistent mass performs better. We have more confidence in the correctness of the comparison values for this case and hence prefer to draw the conclusions based on it only.

Generally, since the equivalent of about 20 modes will be considered in the later sections, it can be concluded that the 0.5 inch (12.7 mm) module with the consistent mass will be adequate for the frequency range of interest.

1.4 Forced Frequency Spectrum

The dynamic problems of interest can also be viewed in the frequency domain for analysis. In doing this the structure is excited at frequencies that are not necessarily the resonant frequencies and the frequency response of the system is calculated.

PlaDyn was used to perform the conventional finite element analysis for the forced frequency analysis. When damping is present in a structure the equations of motion can be written in matrix form as:

$$[K]\{u\} + [C]\{\dot{u}\} + [M]\{\ddot{u}\} = \{P\} \tag{1.23}$$

where $[K]$ is the stiffness matrix, $[C]$ is the damping matrix, $[M]$ is the mass matrix, $\{u\}$ is the nodal displacement vector, and $\{P\}$ is the applied load vector. The frequency domain form of this becomes

$$\Big[[K] + i\omega[C] - \omega^2[M]\Big]\{\hat{u}\} = \{\hat{P}\} \quad \text{or} \quad [\hat{K}]\{\hat{u}\} = \{\hat{P}\} \tag{1.24}$$

where the 'hat' indicates frequency dependent terms. The damping matrix, $[C]$, is assumed to be proportional. This means that $[C]$ can be written as:

$$[C] = \alpha[M] + \beta[K] \tag{1.25}$$

where α and β are constants. We will actually let β be 0 and compute the results for two non-zero levels of damping.

Because of the damping, the dynamic stiffness $[K]$ is complex, consequently the response $\{u\}$ is complex even if the input $\{\hat{P}\}$ is real only. Figures 1.13, 1.14, and 1.15

show the results for values of $\alpha = 0$, 20, 200, and β=0 for all cases. A module size of 0.5 inches (12.7 mm) was used. The range of frequencies span only one resonance. As expected, increasing the damping decreases the response peak and spreads the energy among the other frequency components.

1.5 Modal Analysis

When a system consists of many degrees of freedom, it would be beneficial to reduce the coupled equations of motion to uncoupled algebraic equations. This can be done by applying modal analysis. Modal analysis uses the concept of the modal matrix through which the system can be described in terms of uncoupled equations [5].

As part of an eigenanalysis, we obtain the eigenvectors, one for each eigenvalue or mode. We form the modal matrix by placing these side by side as columns in an array. This modal matrix has some very useful transformation properties when applied to the stiffness, mass, and damping matrices. That is,

$$[\Phi]^T[K][\Phi] = \lceil \tilde{K} \rfloor , \qquad [\Phi]^T[M][\Phi] = \lceil \tilde{M} \rfloor , \qquad [\Phi]^T[C][\Phi] = \lceil \tilde{C} \rfloor \tag{1.26}$$

where $\lceil \tilde{K} \rfloor$, $\lceil \tilde{M} \rfloor$, and $\lceil \tilde{C} \rfloor$ are diagonal matrices. If we represent the displacements as

$$\{u\} = [\Phi]\{\eta\} \tag{1.27}$$

and substitute this into the equations of motion, then after pre-multiplying by the modal matrix allows the coupled equations to be written as uncoupled single degree of freedom systems. The uncoupled system is:

$$\lceil \tilde{K} \rfloor \{\eta\} + [\tilde{C}]\{\dot{\eta}\} + \lceil \tilde{M} \rfloor \{\ddot{\eta}\} = \{\Phi\}_i^T \{P\} \tag{1.28}$$

where $\{\eta\}$ is the vector of modal displacements. Since $\tilde{K}_i = \omega_i^2 \tilde{M}_i$, the above can be written as

$$\omega_i^2 \eta_i + 2\zeta_i \omega_i \dot{\eta}_i + \ddot{\eta}_i = \frac{\{\Phi\}_i^T \{P\}}{\tilde{M}_i} \tag{1.29}$$

where ζ, the damping ratio, is defined as

$$\zeta_i \equiv \frac{C_i}{2\sqrt{K_i M_i}} = \frac{C_i}{2\omega_i M_i} = \frac{\alpha + \beta\omega_i^2}{2\omega_i} \tag{1.30}$$

where ω_i is the modal frequency value. Since less damping is desirable in the higher modes the values for α used were 0, 20, and 200, and β was 0 for all cases.

A standard approach in performing the modal analysis uses the modal displacement method [5]. This method involves solving Eqn. (1.29) for $\{\eta\}$ thereby leading to a solution to the general equation of motion for the displacement, $\{u\}$, and its time derivatives. A second method could also be used to perform the modal superposition. This is the modal acceleration method and involves performing a modal transformation on only the inertia and viscous terms of the equation of motion [12]. This modal transformation yields the following equation

$$\{u\} = [K]^{-1}\{P\} - [\Phi]\lceil\omega^2\rfloor^{-1}(\{\ddot{\eta}\} + \lceil\zeta\rfloor\{\dot{\eta}\}) \tag{1.31}$$

where $\lceil\zeta\rfloor$ is a diagonal matrix with ith diagonal coefficient $2\zeta_i\omega_i$. In this, the matrix multiplication is carried out over only the lowest m eigenvectors and can be approximated as

$$\{u\} \approx [K]^{-1}\{P\} - \sum_{i=1}^{m}\{\Phi\}_i\left(\frac{1}{\omega_i^2}\ddot{\eta}_i + \frac{2\zeta_i}{\omega_i}\dot{\eta}_i\right) \tag{1.32}$$

where m is less than the number of equations of the system. In order to fully solve for $\{u\}$ using the modal acceleration method Eqn. (1.29) is solved for $\dot{\eta}_i$ and $\ddot{\eta}_i$ for i ranging from 1 up to m. This is similar to the solution using the modal displacement method. Eqn. (1.32) is used for superposition to obtain {u} as a function of time [3]. The real advantage in using the modal acceleration method versus the modal displacement method is that in general fewer modes are required for equivalent accuracy. This means that fewer eigenvalues and vectors need be computed thus taking less computational time. However, it does require solving a static problem for the complete system. Generally, this is not a significant difficulty but it does mean that the complete stiffness matrix $[K]$ must be retained. ModDyn [11] is capable of solving it both ways, but in the following only the mode displacement method is used. For very large systems, it is generally less expensive to include higher modes than to retain the stiffness.

The modal displacement method is used by PlaDyn and to account for the effects of the higher modes, the first 20 modes were taken and the center displacement of

the panel was recorded. This number of modes was deemed to be sufficient based on past comparisons.

Computing the forced frequency spectrums using a modal analysis is very efficient since for each mode, we have simply

$$\hat{\eta}_m = \frac{\{\Phi\}_m\{\hat{P}\}}{(\omega_m^2 + \dot{x}\rho_m\omega_m\omega - \omega^2)\tilde{M}_m} \tag{1.33}$$

Figures 1.13, 1.14, and 1.15 show the comparisons with the direct evaluation of the forced frequency response. The results are generally in good agreement even when damping is present.

1.6 Discussion

The static and vibrational results establish the DKT element as accurate; they also give us a set of guidelines to be used when selecting an appropriate mesh size. Generally, for the panel sizes and frequency range of interest here, a module size of about 0.5 inches (12.7 mm) ($\Delta a/a$=0.05) is deemed adequate.

For the modal analysis twenty modes were used to better simulate the panel behavior. It can be seen from the figures that a good agreement exists between the finite element and the modal results for the out-of-plane deflection of the center of the panel. This comparison was performed to establish the relationship between the modal and the FEM method. Depending upon the desired output, and frequency range one method may be more adequate to use over the other. For example, if only a very limited range of frequencies were to be analyzed the FEM method could be used as the computational time would not be a crucial factor. On the other hand, if a broad frequency range was of interest, or even more important, if more than one level of damping was to be analyzed, the modal method would be appropriate. The reason for this is that for the modal method the computationally intensive portion is the subspace iteration. For a given model the subspace iteration need only be performed once. If more than one level of damping was to be analyzed, for example, the actual analysis portion takes only seconds. If more than one level of damping was to be analyzed for the FEM method, for each level of damping a separate analysis would

need to be performed. This would be computationally expensive and in systems with a large number of degrees of freedom is not economically feasible.

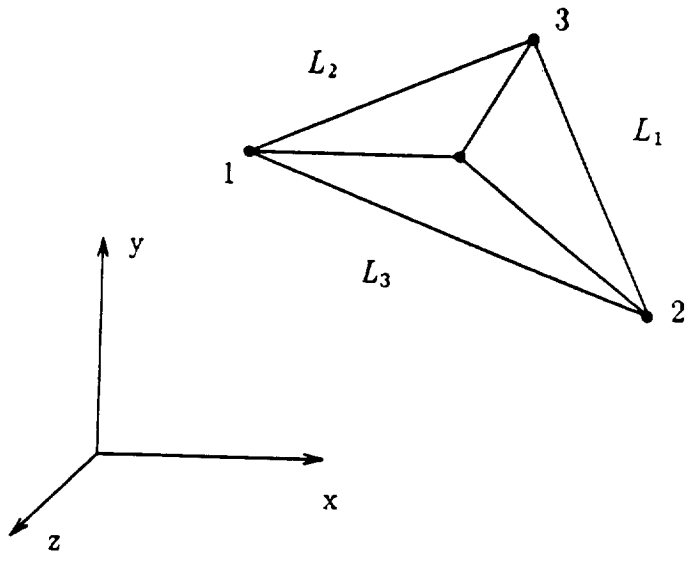

Figure 1.1: Discrete Kirchhoff triangular element with areal coordinates.

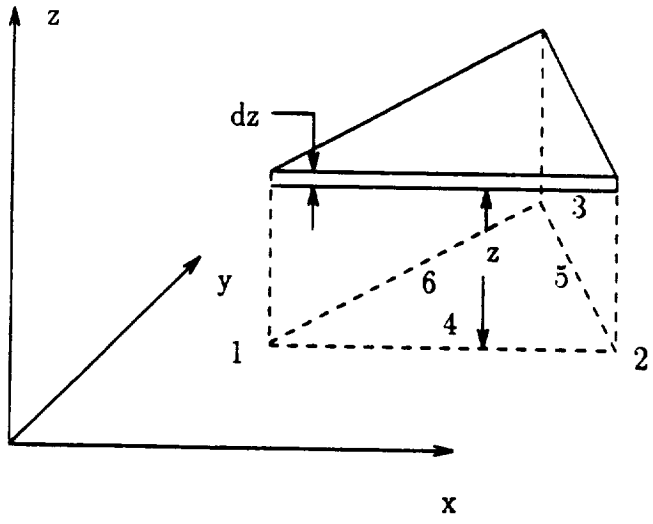

Figure 1.2: Element laminate and nodes.

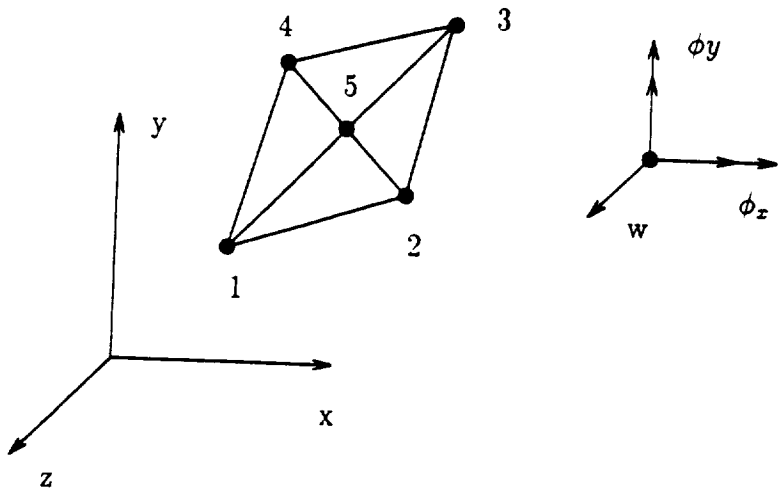

Figure 1.3: A quadrilateral modeled with four triangular elements.

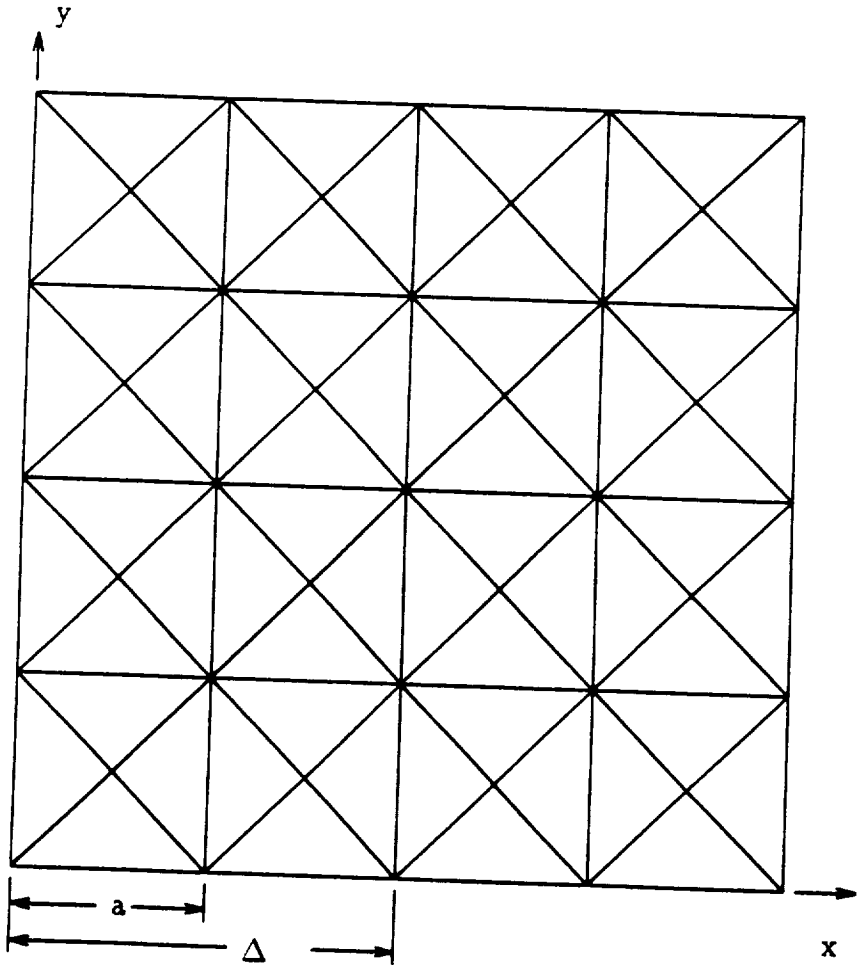

Figure 1.4: Typical finite element mesh.

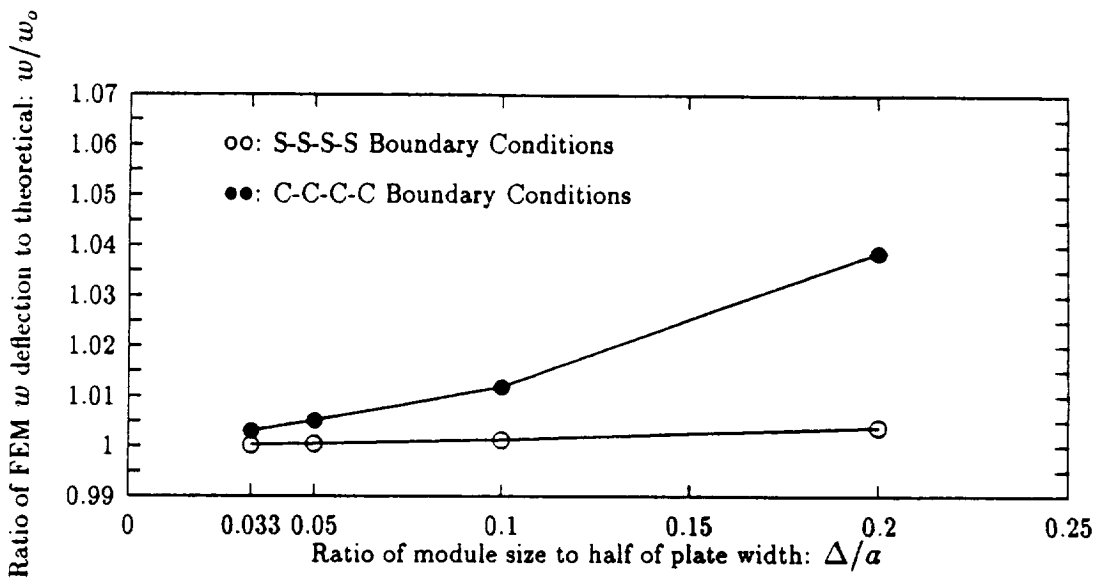

Figure 1.5: Center deflection of a square plate with applied point load.

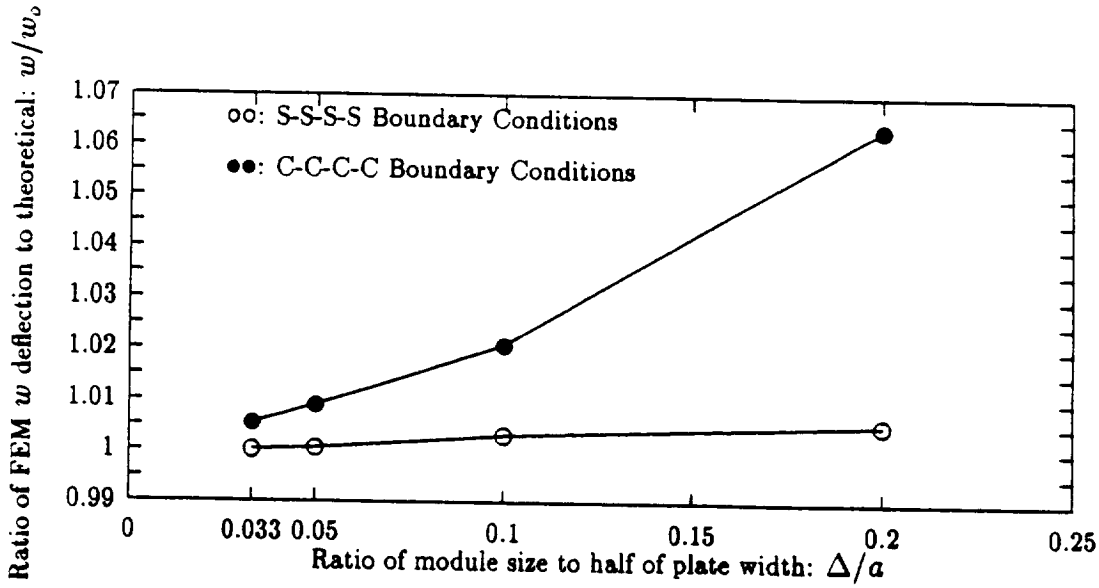

Figure 1.6: Center deflection of a square plate with applied distributed load.

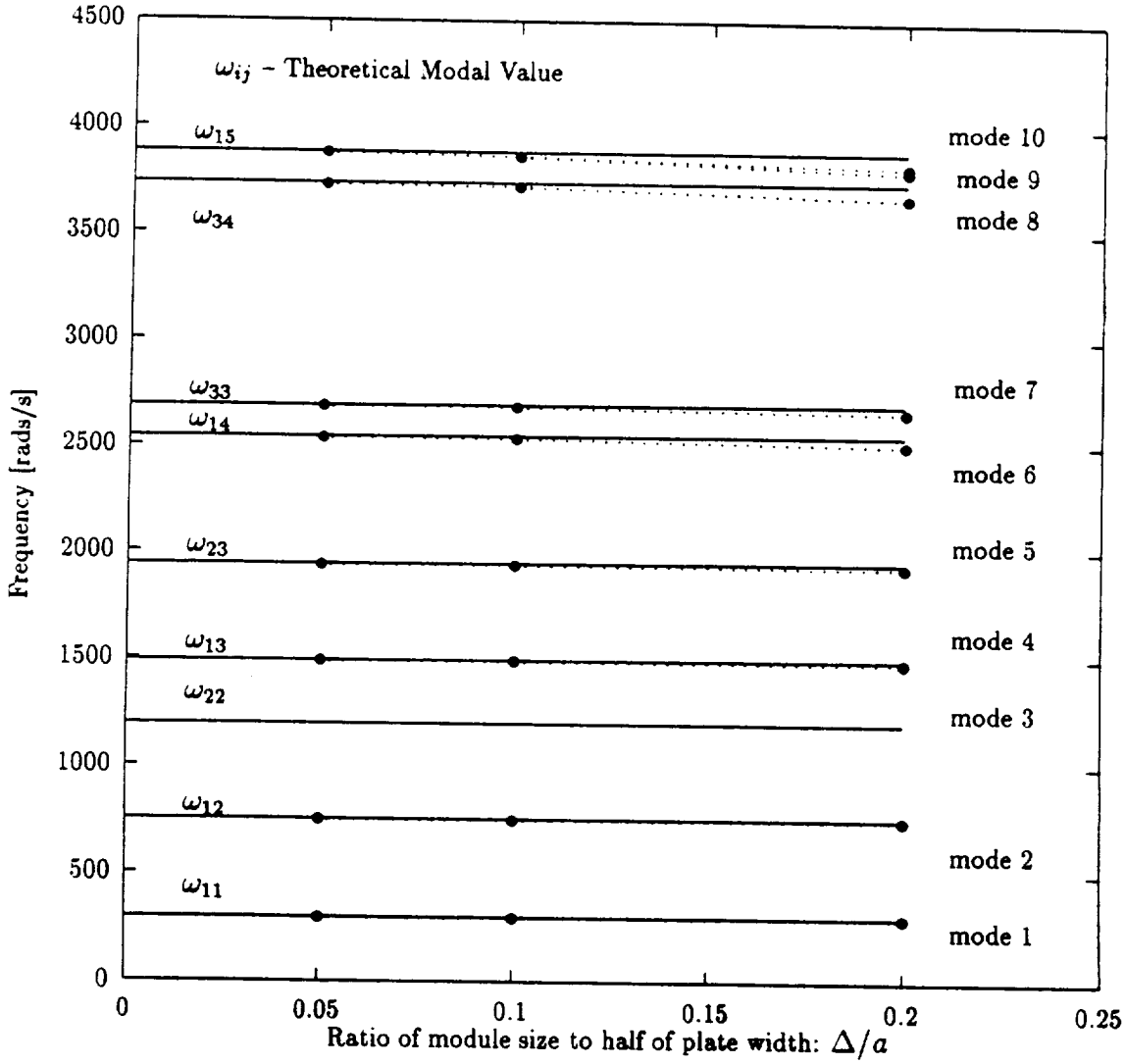

Figure 1.7: Consistent mass matrix comparison for plate with simply supported boundary conditions: modes 1-10.

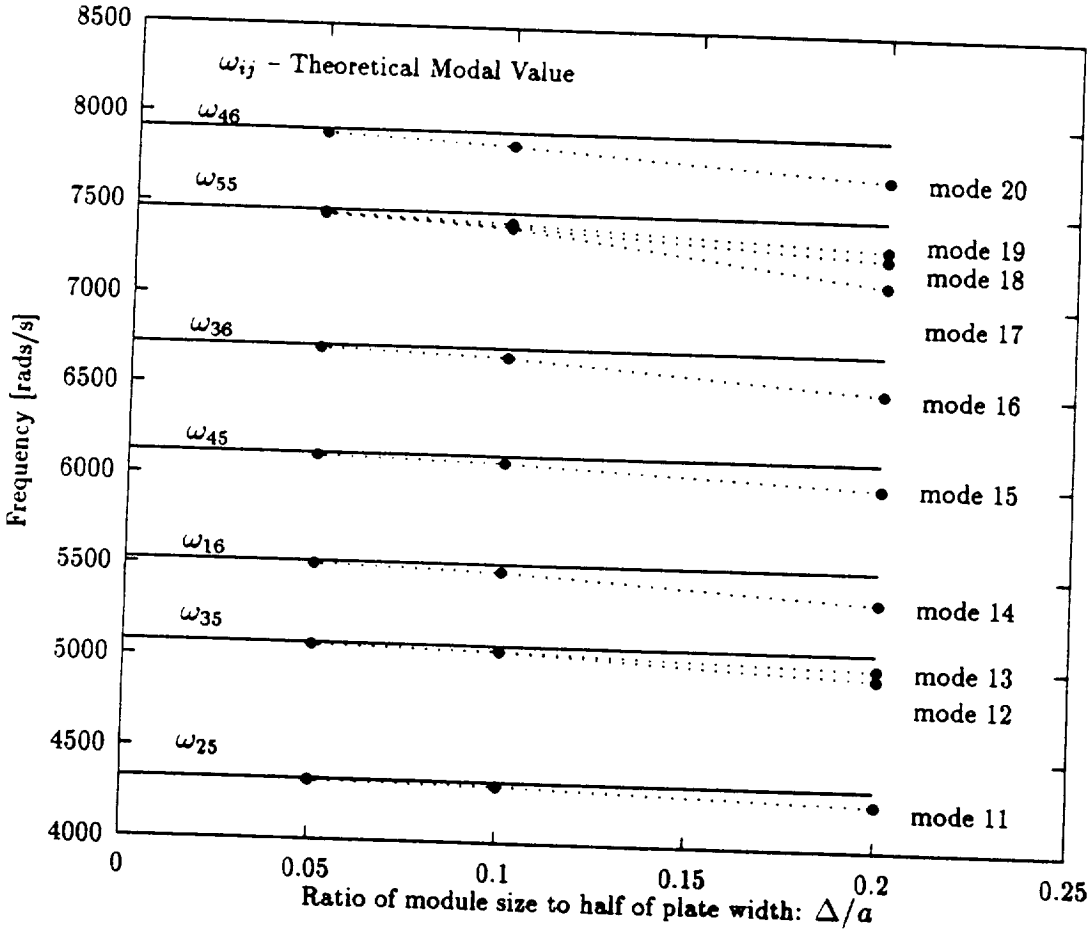

Figure 1.8: Consistent mass matrix comparison for plate with simply supported boundary conditions: modes 11-20.

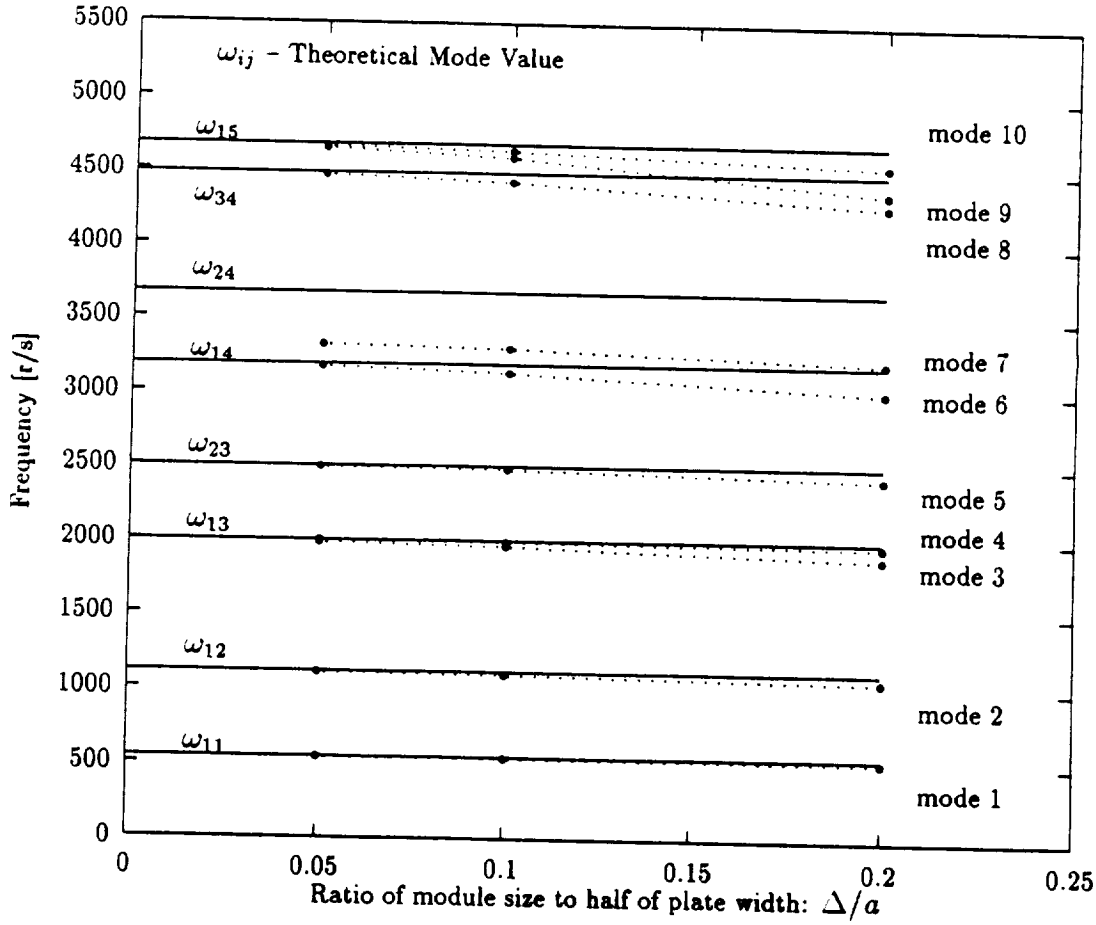

Figure 1.9: Consistent mass matrix comparison for plate with clamped boundary conditions: modes 1-10.

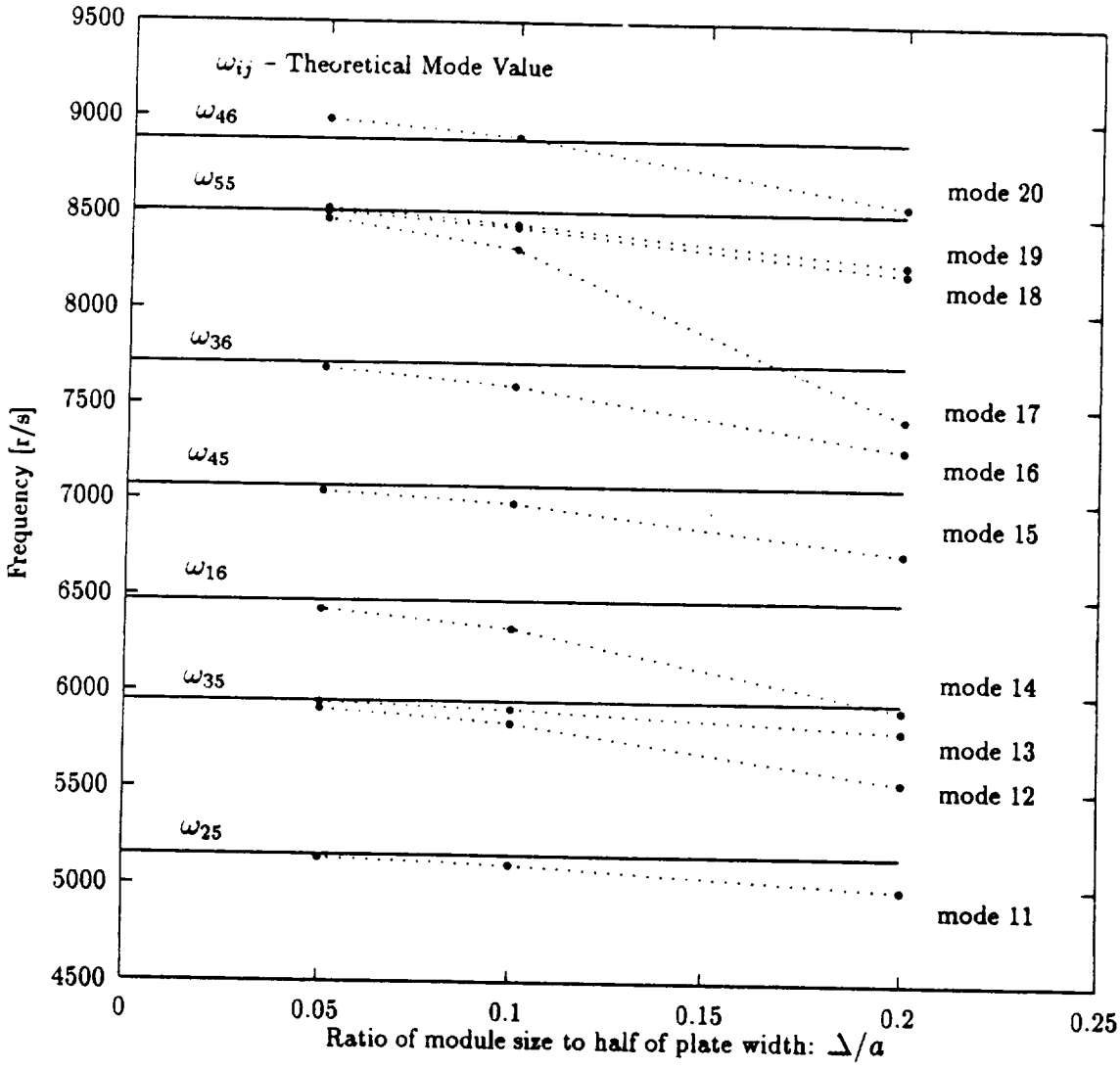

Figure 1.10: Consistent mass matrix comparison for plate with clamped boundary conditions: modes 11-20.

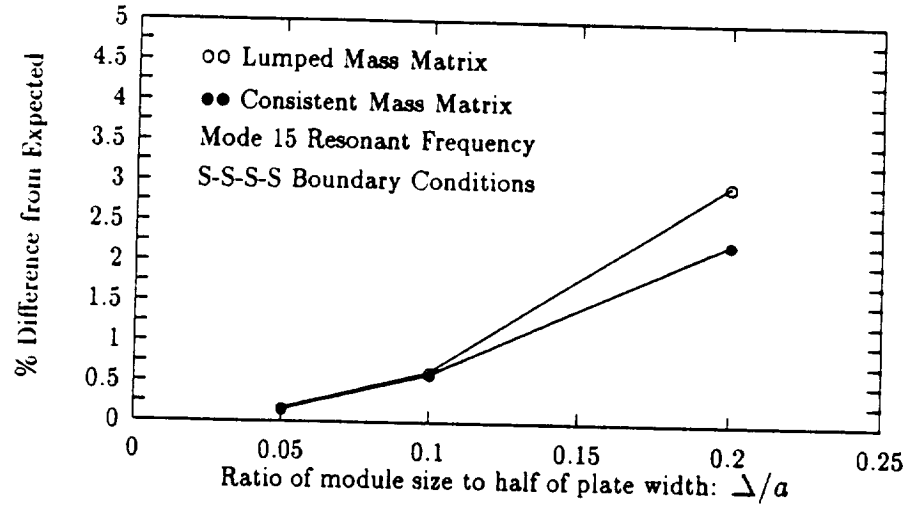

Figure 1.11: Mass matrix comparison for plate with simply supported boundary conditions.

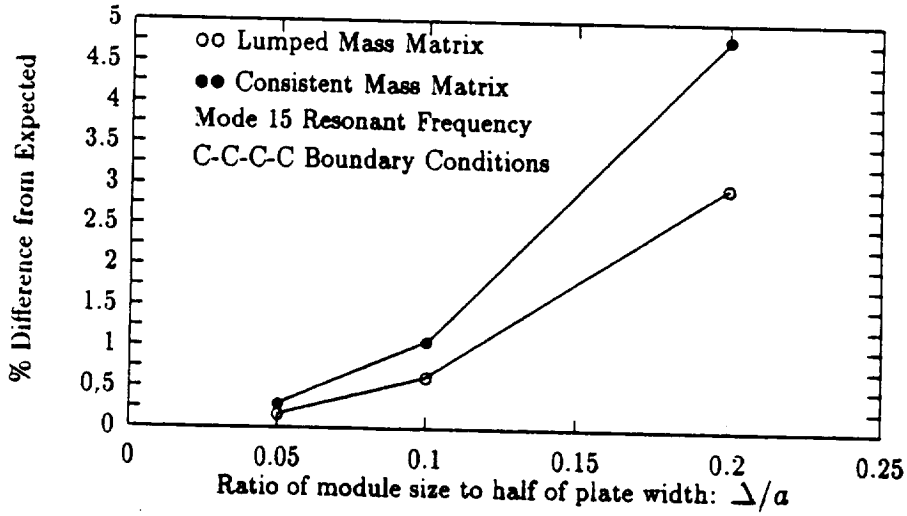

Figure 1.12: Mass matrix comparison for plate with clamped boundary conditions.

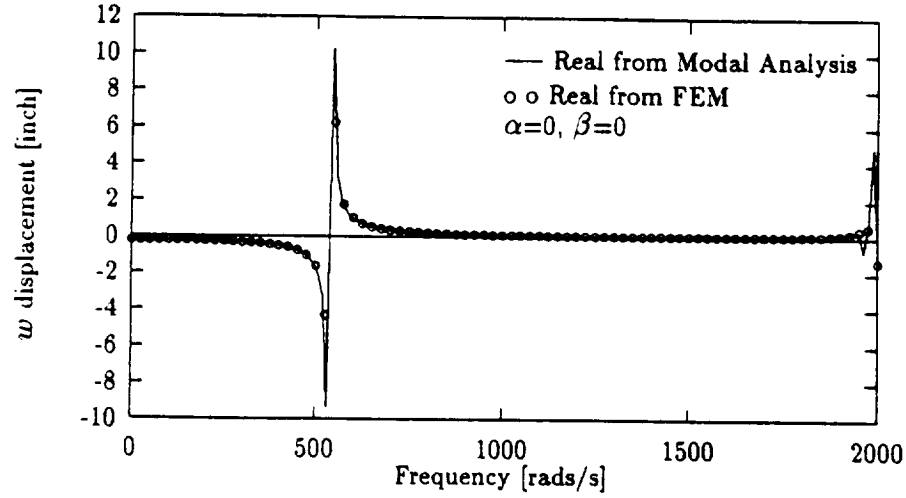

Figure 1.13: Modal and FEM ω displacement spectrum: $\alpha = 0$.

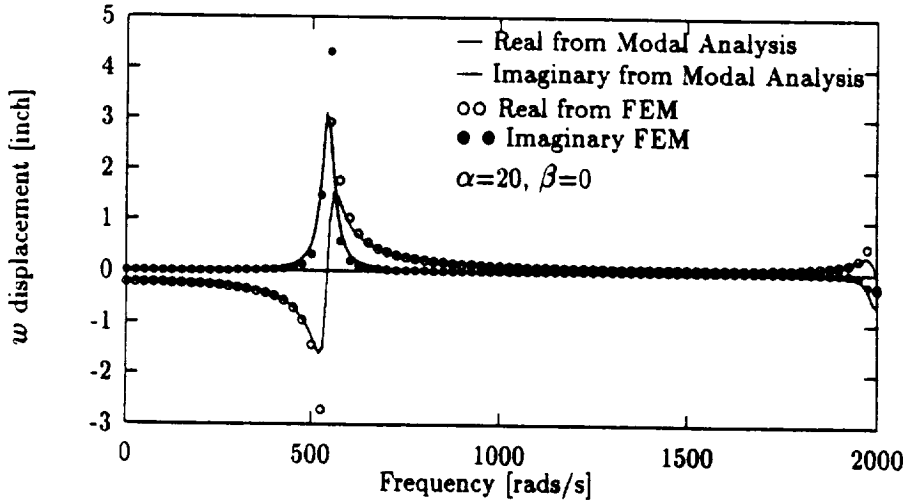

Figure 1.14: Modal and FEM ω displacement comparison: $\alpha = 20$.

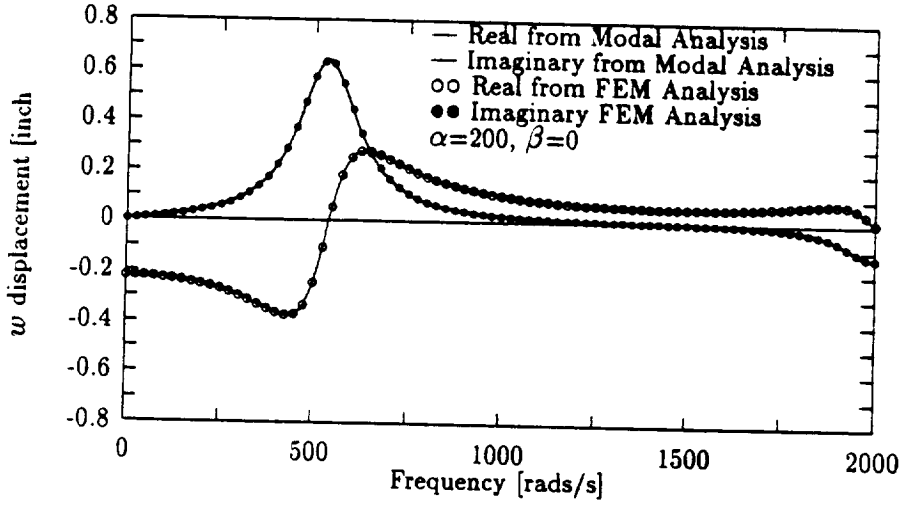

Figure 1.15: Modal and FEM ω displacement comparison $\alpha = 200$.

2. STATIC ANALYSIS OF CRACKED PANELS

Fracture mechanics deals with the conditions under which a body can fail owing to the propagation of an existing crack of macroscopic size. In the analysis of a structure containing a crack the key question to be posed is what load will produce failure for a given crack size, or, for a given loading condition, what will be the allowable crack size. One of the most important quantities for describing or characterizing a crack is the stress intensity factor. This is not a stress concentration factor; the difference being that the former pertains to a singularity in the stress field, whereas the latter pertains to geometries that do not produce infinite stresses [8].

In this section we investigate the accuracy of the finite element modeling as regards the analysis of cracks in a panel. Our objective is to help delimit the parameters of the modeling; that is, establish probable accuracy limits for given meshes and crack sizes.

2.1 Crack in an Infinite Sheet

Consider a through-the-thickness central crack in an infinite plate subjected to uniform remote bending moment, as shown in Figure 2.1; the stress intensity factor, K_I, can be defined according to the maximum tensile stress as

$$K_I \equiv \lim_{r \to 0} \sqrt{2\pi r}\, \sigma_{yy}(r, 0, \frac{h}{2}) \tag{2.1}$$

For this plate bending problem, K_I can be expressed as [19]

$$K_I = K_o = \sigma_o \sqrt{\pi a}\,, \qquad \sigma_o = \frac{6M_o}{h^2} \tag{2.2}$$

where M_o is the applied uniform moment, a is half the crack length, and h is the plate thickness. In this way, the stress intensity due to bending can be viewed analogous to

the in-plane case: we consider the entire surface to be subjected to a remote tensile loading σ_o. However, plates experience plane strain, hence we will use the analytical stress intensity factor, K_o, as given by

$$K_o = \frac{6M_o\sqrt{\pi a}}{h^2} \tag{2.3}$$

This equation was used by Rook and Cartwright in Reference [17] to establish a relationship between K_I/K_o and the ratio of crack length to plate width, $\Delta a/a$.

2.2 Modified Crack Closure Method

The modified crack closure technique, also called the virtual crack closure technique (VCCT), is based on a work-energy principle. Irwin's contention is that if a crack extends by a small amount, Δa, the energy absorbed in the process is equal to the work required to close the crack to its original length [7]. Stated in equation form

$$\begin{aligned} G = &\lim_{\Delta a \to 0} \frac{1}{2\Delta a} \int_0^{\Delta a} \sigma_{yy}(\Delta a - r, 0)\bar{v}(r, \pi)dr \\ &+ \lim_{\Delta a \to 0} \frac{1}{2\Delta a} \int_0^{\Delta a} \tau_{xy}(\Delta a - r, 0)\bar{u}(r, \pi)dr \end{aligned} \tag{2.4}$$

where G is the energy-release rate, σ_{yy} and τ_{xy} are the stresses near the crack tip, $\bar{u}$ and $\bar{v}$ are the relative sliding and opening displacements between points on the crack faces, and Δa is the crack extension at the crack tip. In the above, the first term on the right hand side is the energy release rate for a Mode I crack type and is represented by G_I. The second term in the above is the energy release rate for a Mode II crack type and is represented as G_{II}. The approach for evaluating G_I and G_{II} is based on nodal forces and displacements. In terms of finite element nodal forces and displacements, the expression for G_I and G_{II} can be approximated as [18]

$$G_I = \lim_{\Delta a \to 0} \frac{1}{2\Delta a} \bar{F}_{y_a}(v_b - v_c) \tag{2.5}$$

$$G_{II} = \lim_{\Delta a \to 0} \frac{1}{2\Delta a} \bar{F}_{x_a}(u_b - u_c) \tag{2.6}$$

where Δa is the distance from the crack tip to the next closest node going into the crack. Figure 2.3 shows the position of the points b and c relative to the crack tip,

point a. The attractiveness of this method is that the required parameters are few in number and can be obtained from a single analysis. The latter is important for dynamic analyses.

The above expressions for the energy release rate are based on in-plane displacements. For the problem of out-of-plane bending of a panel the expression for G_I can be written as

$$G_I = \frac{M_{xa}(\phi_{xb} - \phi_{xc})}{2\Delta a} \tag{2.7}$$

where M_{xa} is the moment about the crack axis on the crack tip, ϕ_{xb}, and ϕ_{xc} are the x-rotations of the nodes closest to the crack tip going into the crack.

For the problem of out-of-plane bending being considered, the stress intensity factor, K_s, for the finite element static case was calculated using the following [23]:

$$K_s = \sqrt{\frac{3(3+\nu)EG}{(1+\nu)h}} \tag{2.8}$$

The program PlaDyn was modified so that it could output these parameters directly.

2.3 Effect of Module Size

In order to establish an acceptable model for the cracked panel, calculation of K_s was performed for different module sizes and compared to the handbook values in Reference [17]. The purpose of this comparison is to establish a module size that can accurately model the crack tip and the surrounding nodes. Determining the largest module size was of interest in that a larger module would decrease the amount of disk space required for storage of the mass and stiffness matrices. But more importantly, the computational cost in using a larger module size would decrease thus decreasing actual run time during performing the required analysis.

The cracked panel used in this study is shown in Figure 2.2. The model of the panel was 20 inches (508 mm) wide by 20 inches in length and 0.1 inch (2.54 mm) thick with a center crack. The material properties of Youngs Modulus, E, shear modulus, G, and density, ρ, of the panel were 10.0 msi (69 GPa), 4.0e6 msi (27 GPa), and 2.5E-4 lb/in^3 (6.93 kg/m^3), respectively. Poissons ratio was calculated by $\nu = (E/2G) - 1 = 0.25$. The applied loading consisted of a distributed moment of 10 lb-inches (1.13 N-m).

This distributed moment was applied along the two edges parallel to the crack length which was along the x-axis of the panel. Mid-plane symmetry parallel to the y-axis of the panel was used in order to reduce the amount of disk space required in storing the stiffness matrix. This crack was 4.0 inches in length. The boundary conditions imposed were that the node at the center of the plate on each free edge was restricted in w deflection and ϕ_x rotation.

Calculation of the finite element static stress intensity factor, K_s, for four different module sizes was performed. From Reference [17] the value of K_s was given as $K_o f(a/b)$. In this, a is half of the crack length and b is half of the panel width. In our case we have a/b=0.2 giving $f(a/b)$ of 1.0236 [17]. Using values of M_o=10 lb-inch, a=2.0 inches (5.08 cm), h=0.1 inches (0.254 cm), and ν=0.25, K_o was calculated to be 15792 lb-inch (1784 N-m); giving a value of 16164 (1826 N-m) for K_s.

The K_s value for module sizes of 2, 1, 0.5, and 0.33 inches ($\Delta a/a$=1.0, 0.5, 0.25, and 0.165, respectively) were calculated and Figure 2.4 shows that convergence to the handbook is being achieved. It should be noted however, that the values from the handbook are claimed to be accurate to only about 2 percent.

2.4 Effect of Crack Size

We are interested in establishing the adequacy of the mesh for various crack sizes. To this end, we will keep the module size and panel width constant, and change the crack length. It is expected that as the crack size approaches the module size that significant errors will result.

Meshes containing different crack lengths, a, for a constant panel width, b, were constructed to give different a/b ratios. Figure 2.5 shows the comparison of the computed K_s/K_o values and the values from the handbook for a module size of 0.5 inches. It can be seen from the figure that for small a/b ratios the results deteriorate rapidly. This indicates that for small cracks a finer mesh must be used to model the crack parameters adequately. For a finer mesh model, using modules of 0.33 inches, Figure 2.6 shows the corresponding comparison. For most of the range, the results are better, but again there is deterioration at the small crack sizes.

2.5 Discussion

The difference between the 0.5 and 0.33 inch module established that using a 0.5 inch module size would yield adequate results. Using the 0.33 inch module size would give more accuracy, but the advantage of the slightly better results would be at the expense of the amount of disk space required to store the stiffness and mass matrices. The most important disadvantage would be in the computational run time. For the static case the run time for the 0.5 inch module was approximately 10 minutes. For the case of the 0.33 inch module size it was approximately 18 minutes, or almost 2 times that of the 0.5 inch module size. This computational time difference becomes even more important when a dynamic analysis is performed and the system must be solved at each frequency or time step. Therefore, a module size of 0.5 inches was deemed to give adequate results with regard to the stress intensity factor.

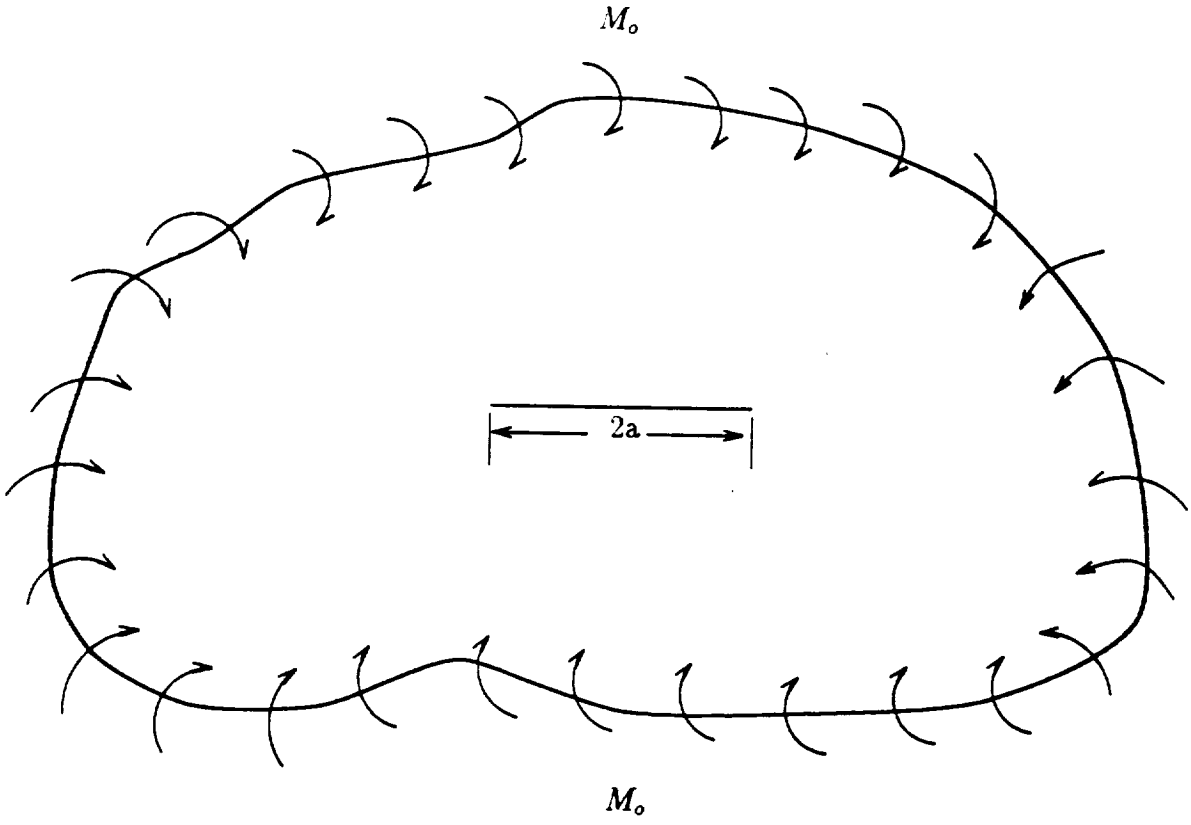

Figure 2.1: Infinite sheet with center crack.

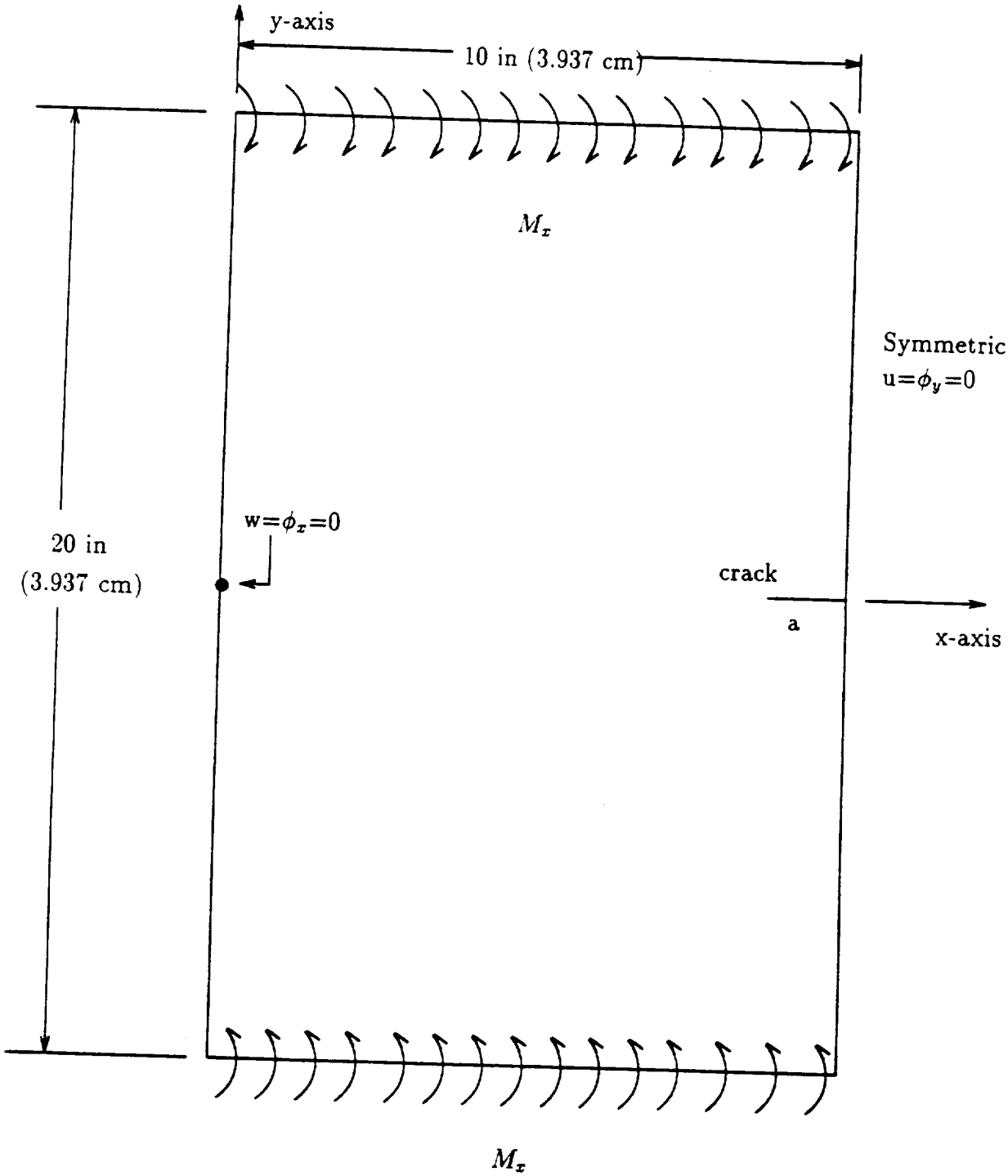

Figure 2.2 Cracked panel model.

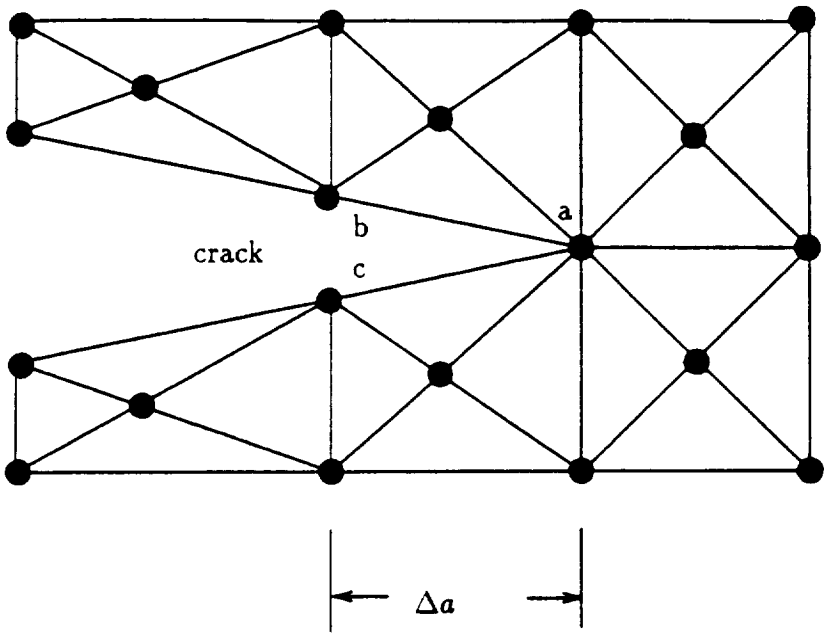

Figure 2.3: Finite element model in vicinity of crack tip.

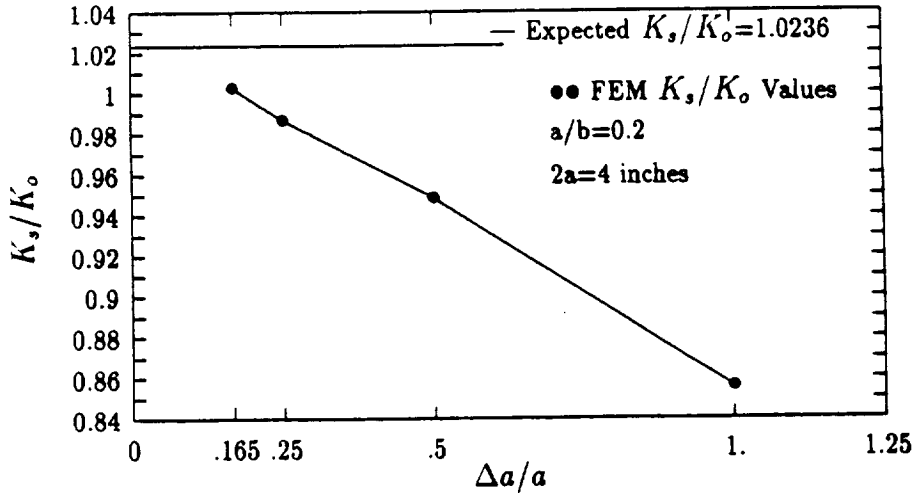

Figure 2.4: Static K comparison versus module size $\Delta a/a$.

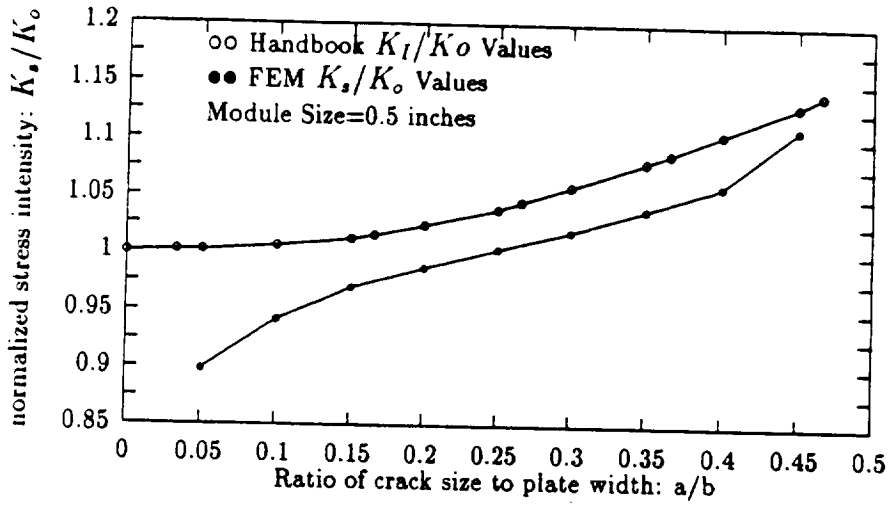

Figure 2.5: Effect of crack size: K_s/K_o comparison with handbook values and 0.5 inch modules.

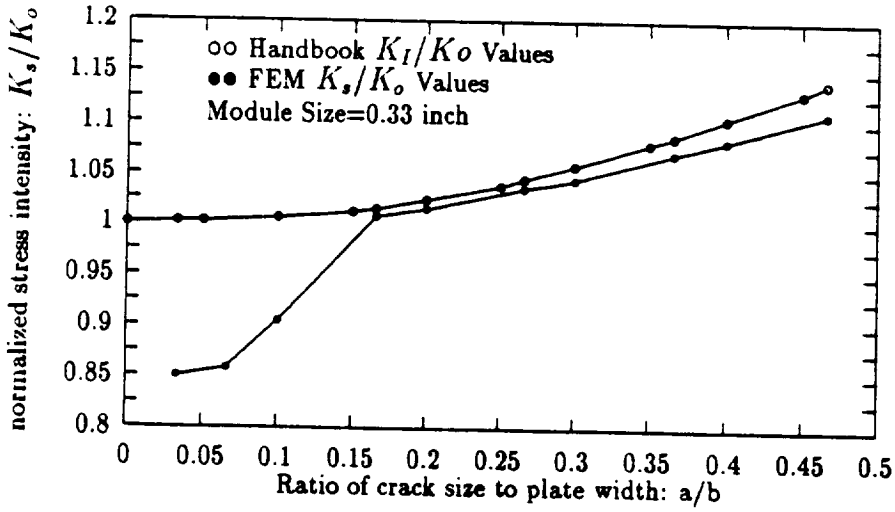

Figure 2.6: Effect of crack size: K_s/K_s comparison with handbook values and 0.33 inch modules.

3. FREQUENCY DOMAIN ANALYSIS OF CRACKED PANELS

Some dynamic analyses are more easily performed in the frequency domain, in particular, the dynamic output for structures that exhibit resonant type behavior is more easily interpreted. It will be shown that the stress intensity factor also exhibits resonant type behavior similar to the structure as a whole.

The stress intensity factor, K, is required in order to perform analysis for fatigue crack propagation. Since various crack geometries need to be considered, a K calibration would be required for each different geometry. This process is expensive in the static case alone but in the frequency domain it is even more so since the calibration must be done over a wide spectrum of frequencies

Two methods for calculating the frequency domain stress intensity factor, $\hat{K}(\omega)$, will be investigated. The first is a variation of the Virtual Crack Closure Technique (VCCT) but applied in the frequency domain to damped systems. The second method combines a modal analysis with a static crack analysis to obtain the variation in the frequency domain. For all of this analysis, one of the restrictions made on the modeling is that the crack is 'open' during vibration. This means that the faces of the crack do not touch during the vibration. This is at least consistent with the general approach to cracks in flexure.

3.1 Forced Frequency Response Analysis

Forced frequency means that the structure is excited at frequencies that are not necessarily the resonant frequencies. One of the primary differences between modal and finite element methods is how the damping is input. The damping for the finite element analysis is taken to be proportional so that we can relate the results to the

modal analysis. When damping is present in a structure, the equations of motion can be written in the frequency domain as

$$\Big[[K] + i\omega[C] - \omega^2[M]\Big]\{\hat{u}\} = \{\hat{P}\} \tag{3.1}$$

The damping matrix, $[C]$, is assumed to be proportional in the form

$$[C] = \alpha[M] + \beta[K] \tag{3.2}$$

where α, and β are constants. In the forced frequency problem we can solve for $\{\hat{u}\}$ over many frequencies. These displacements, which are complex in general, can then be used to obtain the moments and stresses, say, also as a function of frequency. Figure 3.1 shows the displacement of the panel of Figure 2.2 as a function of frequency for medium damping.

The out-of-plane displacement of the crack tip was normalized with respect to its static value. The resonant frequencies are indicated by x marks on the figure. It can be seen that the peaks of the displacement normal occur near the resonant frequency indicating the resonant behavior of the panel. We are interested in characterizing the behavior of the range of about 2000 rads/s, as seen this will include about five resonances.

The finite element and modal analysis for $\hat{\phi}_x$ at the crack tip, was performed for damping values of α of 0, 20, and 200 and a β value of 0 for all cases. The results are shown in Figures 3.2, 3.3, and 3.4. From these figures there is good agreement between the finite element and modal $\hat{\phi}_x$ results. Figure 3.3 shows the spectral behavior of $\hat{\phi}_x$ with medium damping. It exhibits the classical resonance behavior in that the real component goes through a zero while the imaginary component goes through a peak.

A forced frequency modal analysis was also performed for the model in Figure 2.2. The modal analysis package ModDyn was used for this purpose. The system can be written as

$$\omega_m^2\eta_m + 2\zeta_m\omega_m\dot{\eta}_m + \ddot{\eta}_m = \frac{\{\Phi\}_m^T\{P\}}{M_m} \tag{3.3}$$

where ζ, the damping ratio, is obtained as

$$\zeta_m = \frac{\alpha + \beta\omega_m^2}{2\omega_m} \tag{3.4}$$

Figures 3.2 to 3.4 show the results. For the case in which there is no damping present, the results for the two methods discussed show good agreement. When damping is added to the system the comparisons remain in good agreement especially for the lower damping value of α=20. For the higher level of damping value, α=200, the system response exhibited characteristics of being overdamped. Figure 3.4 shows that the agreement was quite good for this case also.

3.2 Virtual Crack Closure Technique

The purpose of this subsection is to modify the concept of the virtual crack closure technique for use in the frequency domain when the response functions are complex.

We can consider all response variables transformed into the frequency domain. In particular, we have for the stress

$$\sigma_{yy}(x,y,t) \Rightarrow \hat{\sigma}_{yy}(x,y,\omega) \tag{3.5}$$

We now take as our definition for the frequency domain stress intensity factor

$$\hat{K}(\omega) \equiv \lim_{r\to 0}\sqrt{2\pi r}\hat{\sigma}_{yy}(r,0,\omega) \tag{3.6}$$

This, in fact could be used as a numerical scheme for K-extraction. It is expected that the value of $\hat{K}$ will be linear (when plotted against $\sqrt{r}$) in the region dominated by the singularity of the crack tip and therefore linear extrapolation to $r = 0$ can be used [9, 15]. In order to use this method a very fine mesh around the crack tip must be used; using a fine mesh makes the analysis computationally expensive, hence this method will not be investigated here. We seek alternative methods.

Irwin's contention is that if a crack extended a small amount, Δa, then the energy absorbed in the process is equal to the work required to close the tip of the extended crack to its original length. This is essentially an equivalency between work done and energy stored. In the frequency domain, all of our quantities are complex and frequency dependent, hence we introduce a complex work term defined as

$$d\hat{W} \equiv \hat{P}d\hat{u} \tag{3.7}$$

Applying this in a manner analogous to the static analysis we are lead to

$$\hat{K} = \sqrt{\frac{3E(3+\nu)\hat{G}}{(1+\nu)h}}, \qquad \hat{G} = \frac{\hat{M}_x \Delta\hat{\phi}_x}{2\Delta a} \tag{3.8}$$

where $\hat{M}_x$ is the resultant moment on the crack tip, $\Delta\hat{\phi}_x$ is the difference in x-rotation between the two nodes next to the crack tip on the inside of the crack, both of which are obtained at each frequency.

Figures 3.5 to 3.7 show the normalized stress intensity factors obtained this way. Not surprising, they show the same general characteristics as the response plots. Again, PlaDyn was modified so that it could output, directly, the complex nodal forces and displacements.

3.3 Global Response Spectrum Method (GRSM)

Reference [15] related a modal analysis method to a baseline extrapolation scheme as giving accurate results for K calculation in the frequency domain. The modal method is useful when a broad spectrum of frequencies is considered. One drawback it has is that when only a limited number of frequencies are of interest. For the modal method to be used, subspace iteration must be performed prior to the modal analysis. This can be computationally expensive for large systems.

The modal analysis approach we discuss has as its fundamental tenet, the idea that the global dynamics are separate from the local crack tip behavior. As shown previously, irrespective of the presence of cracks, the responses can be written as

$$\{\hat{u}\} = [\Phi]\{\hat{\eta}\} \tag{3.9}$$

Since the stresses are related to the nodal degrees of freedom, then we have

$$\{\hat{\sigma}\} = [E]\{\hat{u}\} = [E][\Phi]\{\hat{\eta}\} \tag{3.10}$$

where $[E]$ is understood to be a matrix of elastic constants. If we now take the definition of stress intensity factor as a limit on the σ_{yy} stress, that is,

$$\hat{K}(\omega) \equiv \lim_{x\to 0} \hat{\sigma}_{yy}(x, y=0, \omega) \tag{3.11}$$

we see that we must have

$$\hat{K}(\omega) = \gamma[\phi]\{\hat{\eta}\} \tag{3.12}$$

where γ is some constant. In other words, $\hat{K}(\omega)$ must exhibit the same type of modal behavior as all the other quantities.

We can obtain γ from a static analysis (i.e., the special case when ω=0) and are thus lead to

$$\hat{K}(\omega) = K_s \frac{\hat{\phi}(\omega)}{\phi_o(0)} = \frac{K_s}{\phi_o} \sum [\Phi]\{\eta\} \tag{3.13}$$

where $\hat{\phi}(\omega)$ is a significant response function, ϕ_o is its static value, and K_s is the static stress intensity value. We can obtain K_s from a handbook such as Reference [17] if it is available. In our case, we have

$$K_s = K_o f(a/b), \quad K_o = \frac{6M_o\sqrt{\pi a}}{h^2} \tag{3.14}$$

where M_o is the applied moment. Alternatively, we can obtain K_s directly from a static analysis as was done here.

The stress intensity spectrums are shown in Figures 3.5, 3.6, and 3.7 for damping values of α = 0, 20, and 200, respectively. In general, they follow closely the results from the virtual crack closure technique.

3.4 Discussion

In general, the results of the virtual crack closure technique and the global response spectrum method were in good agreement. This conclusion is important. Since both methods give equivalent results then we have a greater freedom in choosing a method for a particular problem. For example, if only a limited range of frequencies are to be analyzed, the virtual crack closure method could be used. On the other hand, if a broad frequency spectrum is of interest (which would be the case if time reconstructions are to be performed) the modal method would be appropriate. For the modal method the computationally intensive portion is the eigenanalysis and this cost can be distributed over the large number of frequencies. The cost of the actual modal summation portion is insignificant. The direct forced frequency solution using finite elements does not enjoy such a speed up, as each frequency calculation is independent.

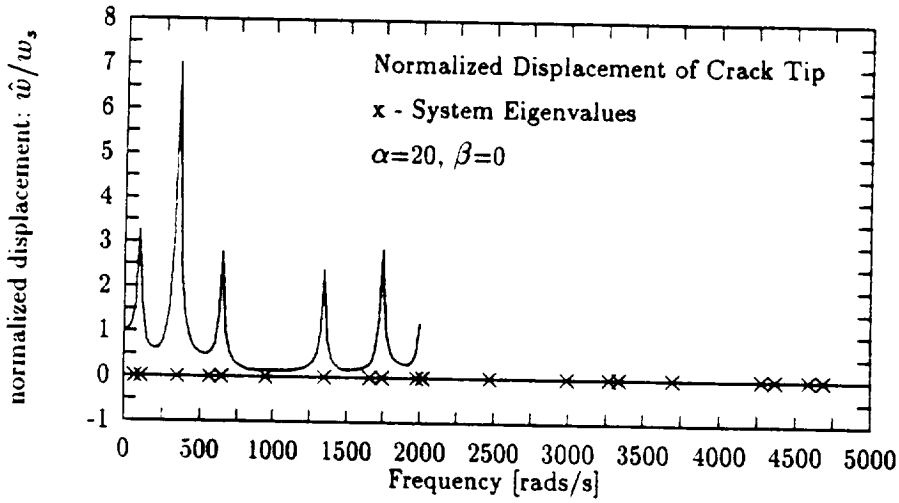

Figure 3.1: Resonant behavior of cracked panel: $\alpha = 20$.

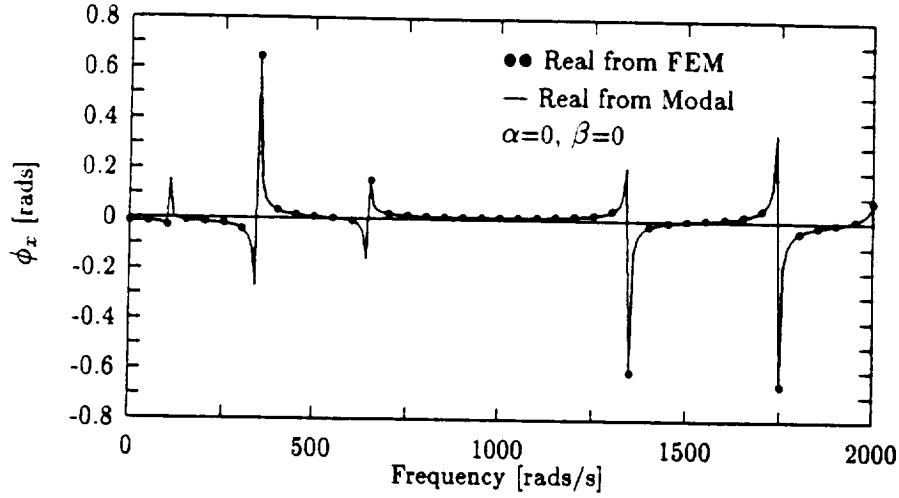

Figure 3.2: $\hat{\phi}_x$ spectrum with no damping.

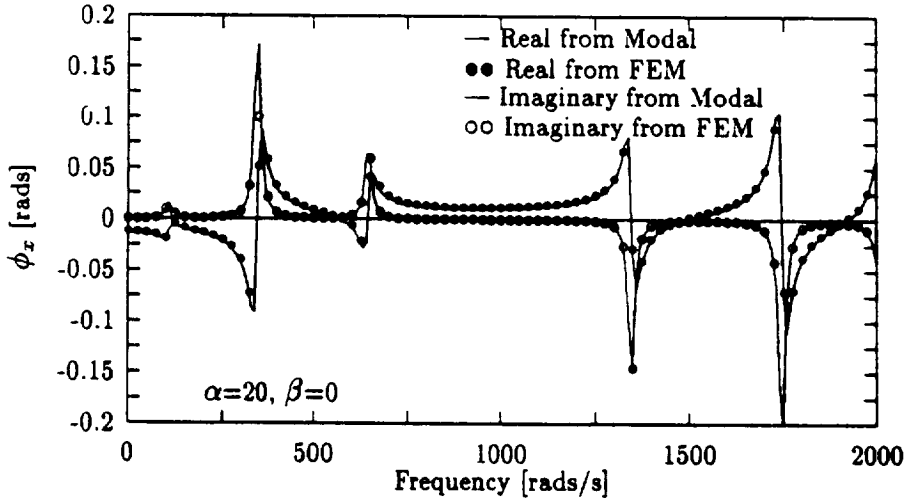

Figure 3.3: $\hat{\phi}_x$ spectrum with medium damping.

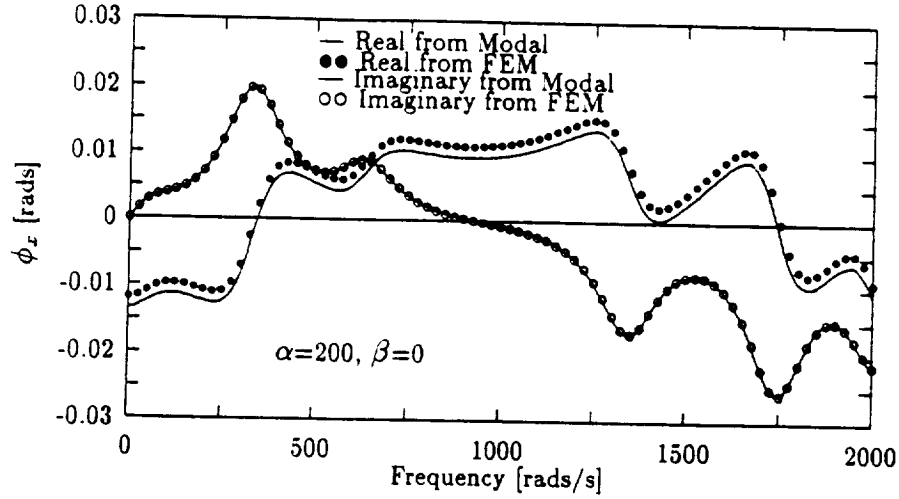

Figure 3.4: $\hat{\phi}_x$ spectrum with high damping.

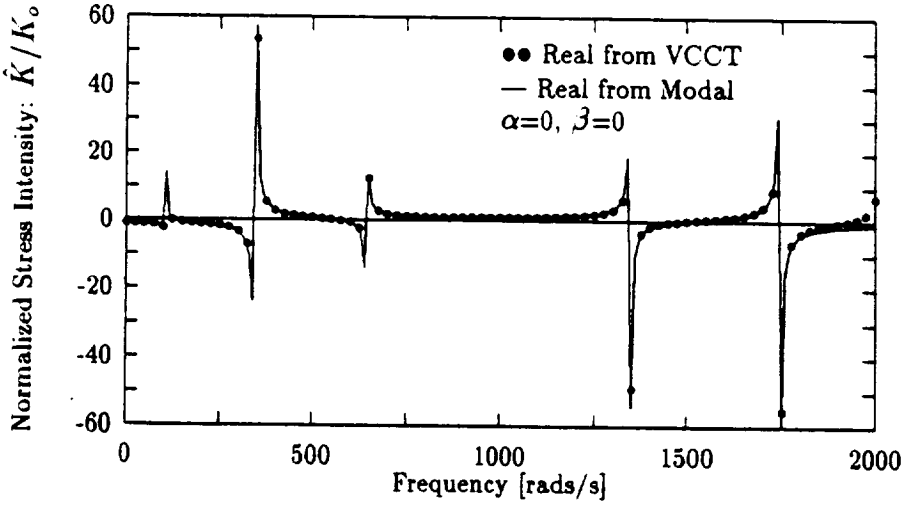

Figure 3.5: $\hat{K}$ spectrum with no damping.

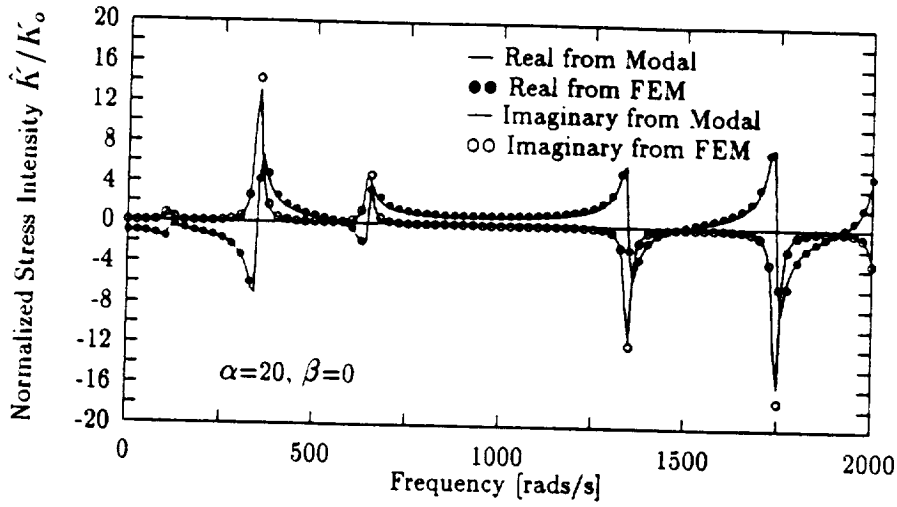

Figure 3.6: $\hat{K}$ spectrum with medium damping.

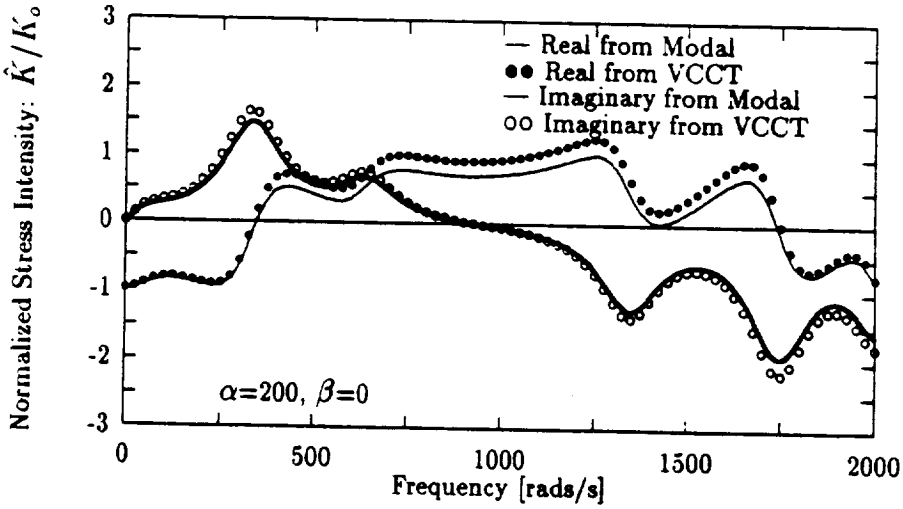

Figure 3.7: $\hat{K}$ spectrum with high damping.

4. TRANSIENT RESPONSE OF CRACKED PANELS

If a structure is excited by a suddenly applied, short term, excitation the response is said to be a transient or impact response. After the force has stopped the structure will then eventually exhibit free vibrations. If damping is present the vibrations will then decay over time.

In this section we are interested in determining the time history response of a panel with a crack. The first method uses direct time integration of the system of equations. This was performed using PlaDyn. The second method uses modal summation. The modal analysis was performed using the modal analysis package ModDyn. The third technique uses a spectral approach where frequency response functions are first obtained and then transformed to the time domain by the inverse fast Fourier transform (FFT).

4.1 Finite Element Transient Analysis

For the transient analysis of the panel, the equations of motion are written as

$$[K]\{u\} + [C]\{\dot{u}\} + [M]\{\ddot{u}\} = \{P\} \tag{4.1}$$

The applied force {P} is a function of time and is written as $\{P\}(t) = \{p\}P(t)$, where $\{p\}$ is a vector representing the time independent distribution of forces. For the panel as used in the previous section, say, {p} consists (mostly) of unit moments applied at each top and bottom boundary node. P(t) is the input function of time and is shown in Figure 4.1 and its amplitude spectrum is shown in Figure 4.2.

In performing the finite element transient analysis, eqn. 4.1 was time integrated using Newmark implicit time integration. For the integration the time step was chosen to be $50\mu s$ with 400 time steps giving a time window of 0.02 seconds.

The transient finite element results from PlaDyn for the rotation are shown in Figures 4.3, 4.4, and 4.5, for damping values of 0, 20, and 200 for α, with β being 0 for all cases. It is seen that the effect of damping is noticeable only at the long time. The initial transient response settles into a vibration with what appears to be two dominant modes.

The time domain transient K value, K_t, was calculated by using the virtual crack closure technique already discussed in Section 2. We use the formulas

$$K_t = \sqrt{\frac{3E(3+\nu)G}{(1+\nu)h}}, \qquad G = \frac{M_x \Delta\phi_x}{2\Delta a} \tag{4.2}$$

directly, using G and M_x at each time step. This method is very convenient for transient analysis because it requires monitoring only a few parameters; namely, the rotations of the nodes closest to the crack tip and the moments at the crack tip. Figures 4.6, 4.7, and 4.8 show the time histories for the stress intensity factor. As expected, they seem to follow the rotation responses very closely. It is worth pointing out that PlaDyn obtains these results as a post-processing operation. That is, during the transient analysis, only the nodal displacements are stored. Later, these are re-read into the program to selectively give other quantities such as stresses or forces by combining with the element stiffness relation.

We can consider these transient finite element results to be our baseline results for comparison with the modal analysis and spectral analysis results.

4.2 Transient Modal Analysis

Rather than integrating the coupled equations of motion, the transient modal analysis uses the modal matrix to first transform these into a set of uncoupled single degree of freedom equations. This set of equations is represented as

$$\tilde{K}_i \eta_i + \tilde{C}_i \dot{\eta}_i + \tilde{M}_i \ddot{\eta}_i = \tilde{P}_i \tag{4.3}$$

where the quantities $\tilde{K}_i$, $\tilde{C}_i$, $\tilde{M}_i$ are the modal stiffness, damping and mass modal matrices, respectively, and η_i are the modal coordinates. This equation is integrated using Newmark implicit time integration to find $\eta(t)$, $\dot{\eta}(t)$, and $\ddot{\eta}(t)$ for each mode.

Again, as for the finite element analysis, the time integration step used was $50\mu s$ with 400 time steps. The separate modes are then recombined to give the actual response as

$$\{u\}(t) = [\Phi]\{\eta\}(t) \tag{4.4}$$

where $\{u\}(t)$ is the displacement vector corresponding to the original finite element analysis. The advantage of this approach is that it allows the selection of the range of modes that participate in the response—these are generally much lower than the system size. Initially, 20 modes were used for the analysis. But, based on later results the number of modes was increased to 30. Increasing the number of modes takes into account more of the structure; thus making the results better.

A transient analysis using modes in the summation was performed. Figures 4.3, 4.4 and 4.5 show the comparison between the modal and finite element results for ϕ_x. The comparisons are seen to be good. This is to be expected since both methods employ the same discretization of the system and the same integration scheme of Newmark implicit time integration. Hence as long as the number of modes is adequate, the correspondence should almost be exact.

The K_t calculation for the modal analysis was based on the same VCCT equation as the finite element analysis. The one difficulty with this formulation is that the moment on the crack tip is needed. Since the modal analysis calculates displacement responses of the system only, a scheme had to be devised to obtain the force on the crack tip associated with the displacements. We did this by using ModDyn to create the post-processing file of displacements for use by PlaDyn. PlaDyn was then used to perform the force history analysis based on these modal displacements.

Figures 4.6, 4.7, and 4.8 show the comparison with the finite element results. Again, as expected the agreement is very close.

4.3 Spectral Analysis

When the response of a given panel due to different loading histories is required, a transient analysis for each loading must be performed. For a system with a large number of degrees of freedom this is computationally expensive. Spectral analysis

is a scheme that can be used to avoid this by allowing convenient frequency domain convolutions with the applied force. This is illustrated here.

In spectral analysis, a time history is given the representation [4]

$$u(x_1, y_1, t) = \sum \hat{u}_n(x, y, \omega_n)(\omega)e^{i\omega_n t} \tag{4.5}$$

where $u(t)$ is the time response, $\hat{u}_n$ is the spectrum of amplitudes, and ω_n are the frequencies. In the frequency domain, the response due to a load can be written as

$$\hat{u} = \hat{H}_u \hat{P} \tag{4.6}$$

where $\hat{H}_u$ is the transfer function. Once this is known then the simple product above (called a convolution) with a different $\hat{P}$ is used to get the response to different load histories.

The approach is applicable to any response quantity. In particular, the stress intensity history can be obtained from

$$\hat{K} = \hat{H}_k \hat{P} \tag{4.7}$$

where we can identify $\hat{H}_k(\omega)$ as the spectrum in Figures 3.5, 3.6, and 3.7.

We will demonstrate this approach using transfer functions obtained by direct finite element analysis for $\hat{\phi}_x$ and $\hat{K}$, by modal analysis for $\hat{\phi}_x$, and by using the global response spectral method to find $\hat{K}$.

In order to perform the convolution, the force history must be transformed to the frequency domain. This is done by using the fast Fourier transform (FFT). When performing the FFT on the force history two variables, the number of FFT points, N, and the time increment, Δt must be decided upon. One restriction on N is that it must be a multiple of 2; that is 2, 4, 16, 32, and so on. These two variables dictate the total time window and the frequency increment of the components in the frequency domain. For example, using parameters that correspond to the PlaDyn forced frequency results of 1024 points with a time increment of 245.4 μs, would give a total time window of 0.251 seconds, and a corresponding frequency increment of 3.979 hertz or 25 rads/s. The transform of the force history used in the spectral analysis is shown in Figure 4.2.

It has been established in the earlier parts of this section that there is a correlation between the trend exhibited by the rotation ϕ_x and the stress intensity factor. Thus, an initial indication of how closely the stress intensity factor will match the baseline finite element results is achieved by comparing the inverse FFT of the convolution of the force transform and the frequency domain ϕ_x values. The results for this are shown in Figure 4.9, 4.10 for damping values of α=20, and 200, and β=0, respectively.

Initially, the comparison between the finite element inverse FFT rotation values and the baseline finite element rotation values showed some disagreement. This difference was caused by the limited frequency spectrum of the forced frequency finite element results. Only 81 points were taken in the forced frequency finite element analysis because of long computational time. Therefore, when $\hat{H}$ was convolved with the transform of the force a very limited range of the force was used. This was corrected by broadening the spectrum of the finite element forced frequency analysis. When this frequency spectrum was convolved with the force transform more of the force was used; therefore, giving more non-zero points when taking the inverse FFT and giving better results when compared to the baseline FEM results as shown in Figures 4.9 and 4.10.

The $\hat{K}$ values calculated using the broader frequency spectrum values were used as the transfer function and the convolution with the transform of the force was performed. The inverse FFT was taken and the comparison between the results and the finite element baseline results are shown in Figures 4.11, and 4.12 for damping values of α = 20 and 200, respectively, and 0 for β. The K_t values were normalized by using

$$K_{omax} = \frac{6M_o P(t)_{max}\sqrt{\pi a}}{h^2} \tag{4.8}$$

where $P(t)_{max}$ is the peak value of the scaling history shown in Figure 4.1. As expected, the agreement with the baseline finite element results is very close.

The forced frequency modal analysis can be performed at any number of frequency intervals for many frequency steps. This was because once the eigenanalysis, which is the computationally expensive portion of the modal analysis, is done, the modal summation takes a relatively short time to execute. A frequency increment of 10

rads/s was used for 1000 frequency steps. Using this number of frequency steps takes the frequency spectrum out to the Nyquist of the force transform. Taking the modal frequency spectrum out to the Nyquist enables the full force amplitude to be used when the convolution is taken between the modal transfer functions and the transform of the force. The comparison between these results and the baseline finite element transient ϕ_x values are shown in Figure 4.13, and 4.14 for the two damping values. The results were again normalized similarly to the finite element results. The results seem to be very close. In fact they are about the same as obtained in the time integration scheme.

The $\hat{K}$ values found by using the GRSM method were used as the transfer function and convolved with the transform of the force. Figures 4.15, and 4.16 show that the comparison between the GRSM reconstruction values and the baseline finite element results are again in good agreement.

4.4 Discussion

The choice of a particular method for transient analysis depends upon the type of problem to be examined. If, for example, a limited time window is to be examined then the finite element method with direct integration may be used since the number of time steps would be small. On the other hand, if multiple loading histories are to be used or responses over a very long time are required then the modal methods are indicated since only one eigenanalysis would be required. This is mentioned since in the modal analysis this is the part that is computationally intensive. The actual summation portion takes a short amount of time and can be performed for a variety of damping values and force histories.

The use of the spectral method gives an alternative to the two methods mentioned above. In this, a single forced frequency analysis is performed and by convolving with the transform of the applied load and performing an inverse fast Fourier transform, the results in the time domain for different load histories can be found. This method can be very useful if a single model is to be examined over a variety of input load histories. The comparisons shown above illustrate that if an adequate number of

transform points are taken, the spectral method will yield results comparable to those that would be obtained by either method previously mentioned.

We thus have four alternative methods for calculating $K(t)$, the stress intensity factor in the time domain. The choice of using the particular method should be based on problem parameters such as if multiple analysis for the same model, if multiple levels of damping are to considered and the time window of interest.

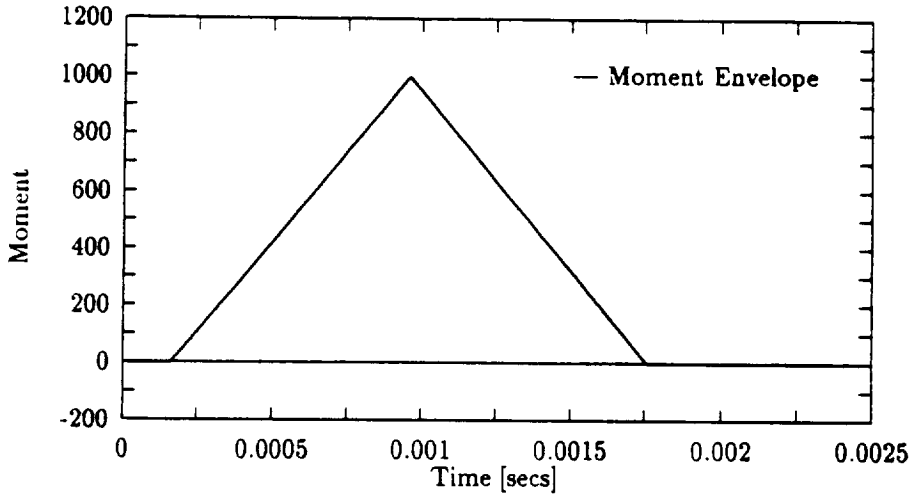

Figure 4.1: Applied load history.

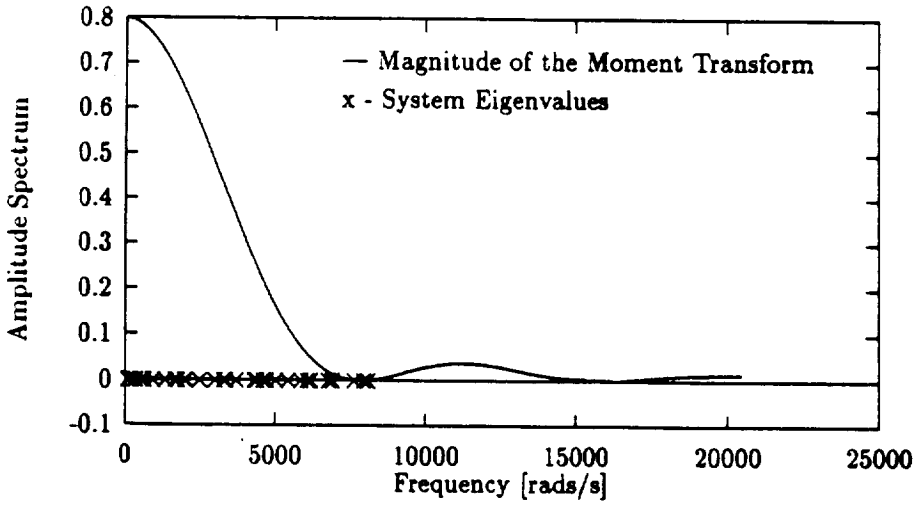

Figure 4.2: Transform of applied load history.

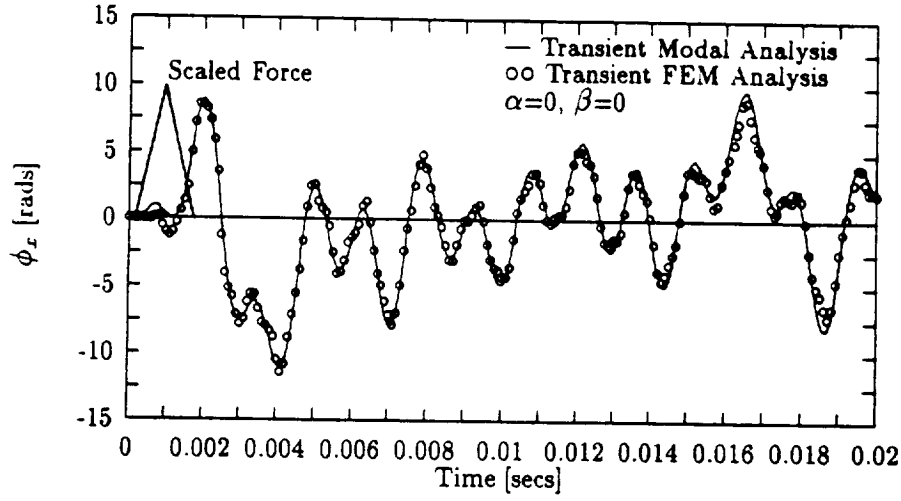

Figure 4.3: Transient modal and FEM ϕ_x comparison: $\alpha = 0$

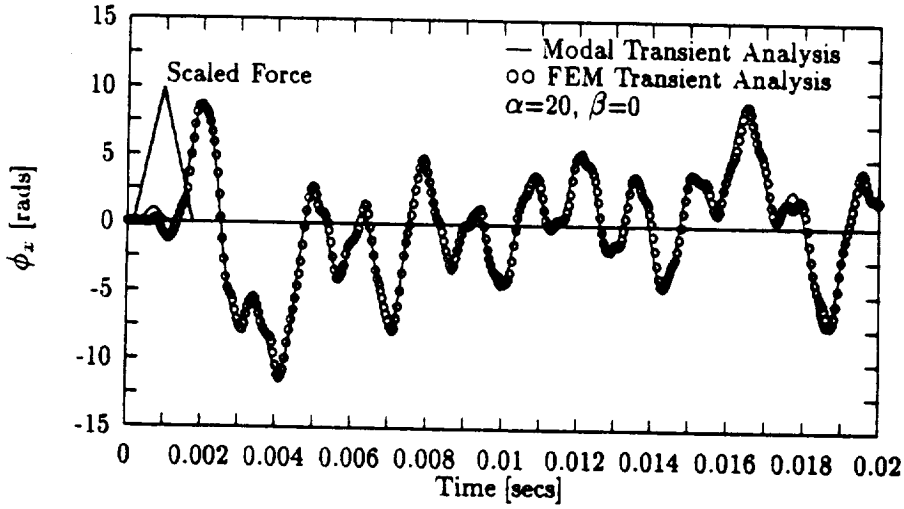

Figure 4.4: Transient modal and FEM ϕ_x comparison: $\alpha = 20$

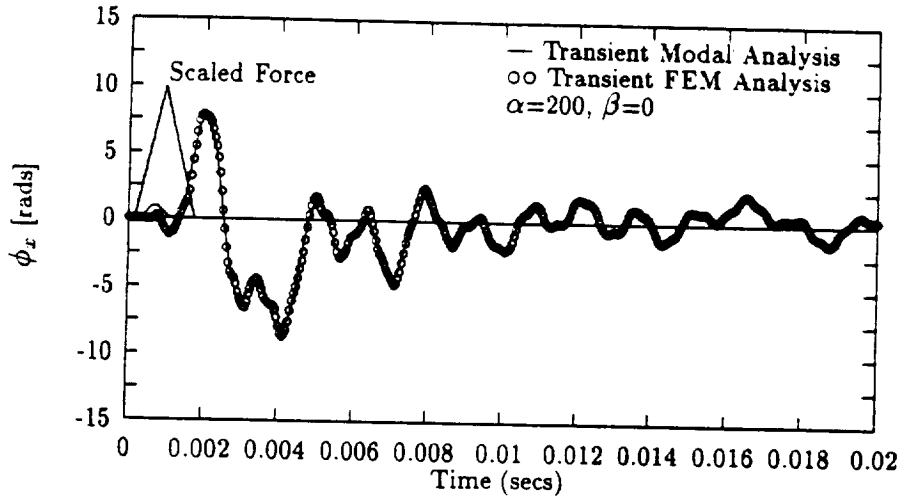

Figure 4.5: Transient modal and FEM ϕ_x comparison: $\alpha = 200$

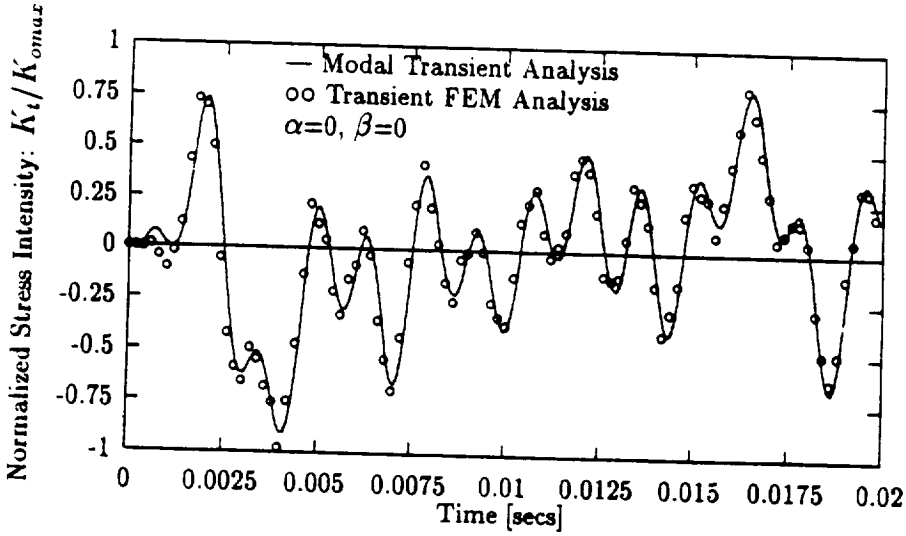

Figure 4.6: Modal and FEM transient K_t/K_{omax} comparison: $\alpha = 0$

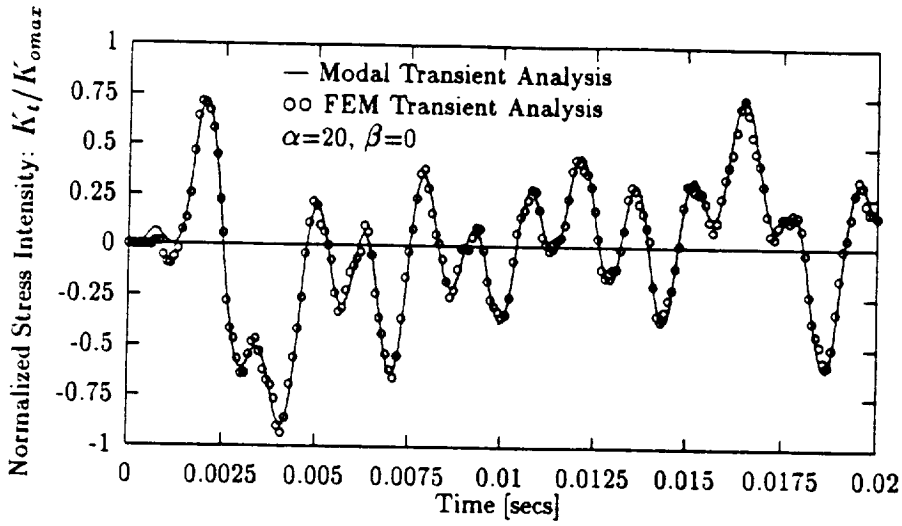

Figure 4.7: Modal and FEM transient K_t/K_{omax} comparison: $\alpha = 20$

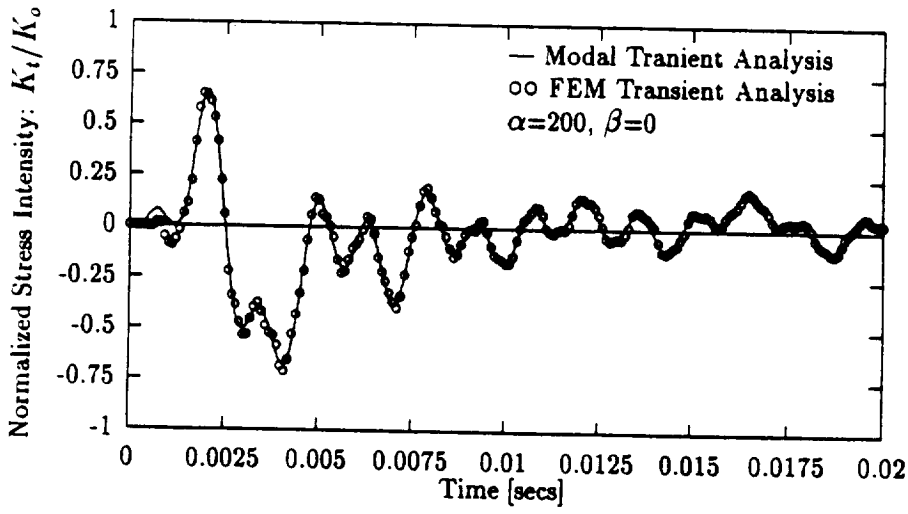

Figure 4.8: Modal and FEM transient K_t/K_{omax} comparison: $\alpha = 200$

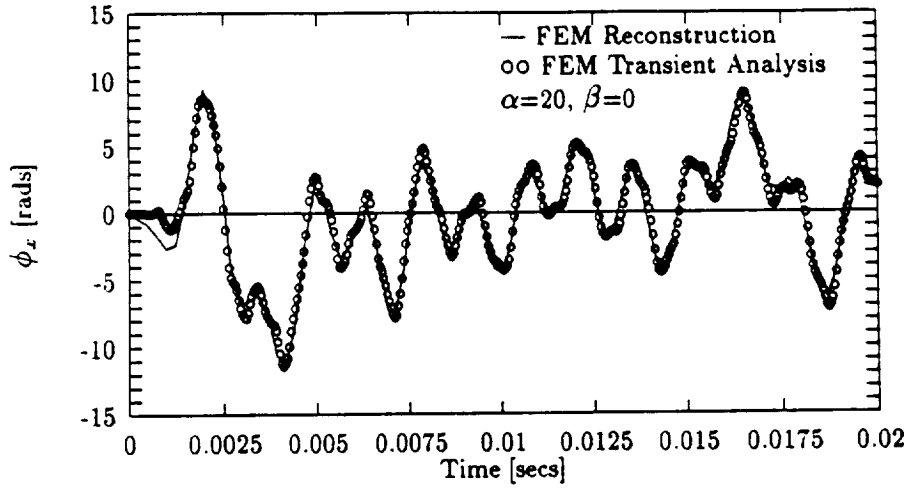

Figure 4.9: FEM transient and FEM reconstruction ϕ_x comparison: $\alpha = 20$

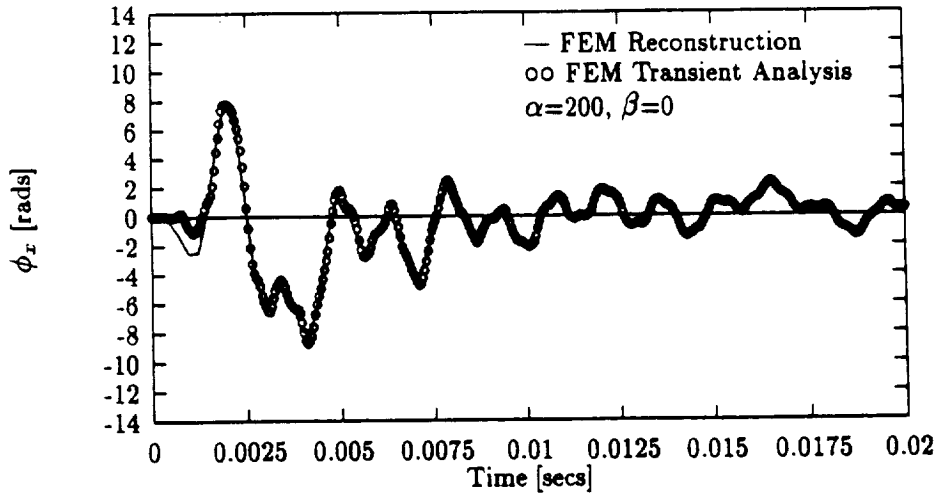

Figure 4.10: FEM transient and FEM reconstruction ϕ_x comparison: $\alpha = 200$

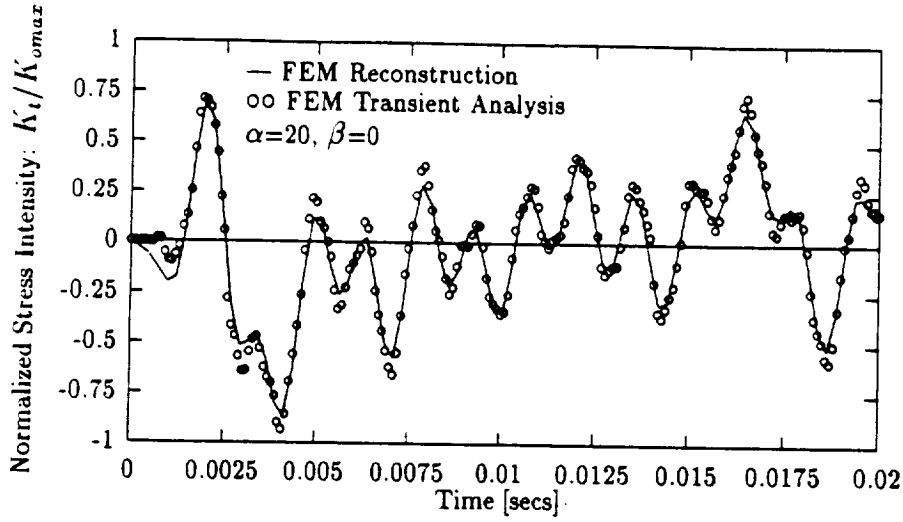

Figure 4.11: FEM transient and FEM reconstruction K_t/K_{omax} comparison: $\alpha = 20$.

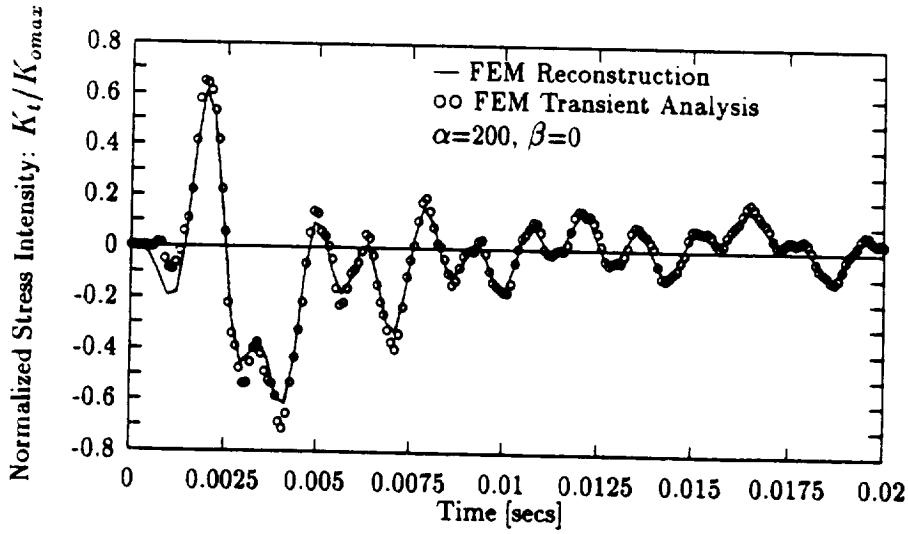

Figure 4.12: FEM transient and FEM reconstruction K_t/K_{omax} comparison: $\alpha = 200$.

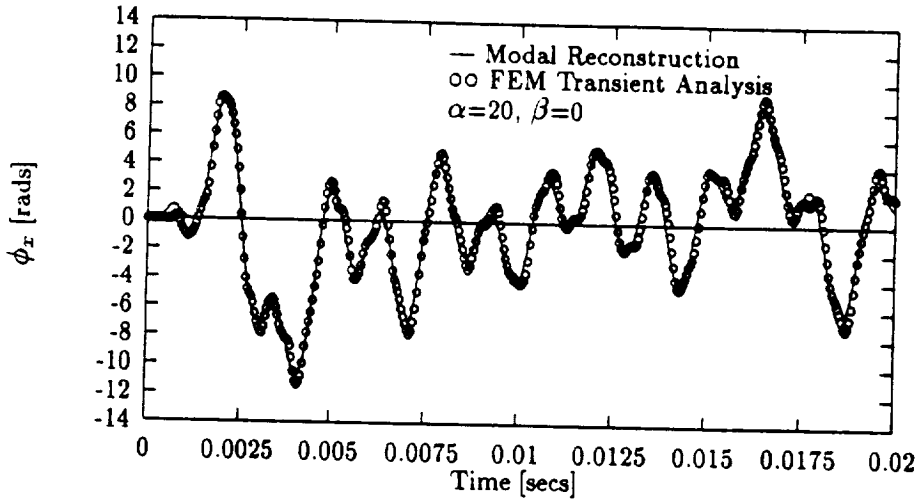

Figure 4.13: FEM transient and modal reconstruction ϕ_x comparison: $\alpha = 20$

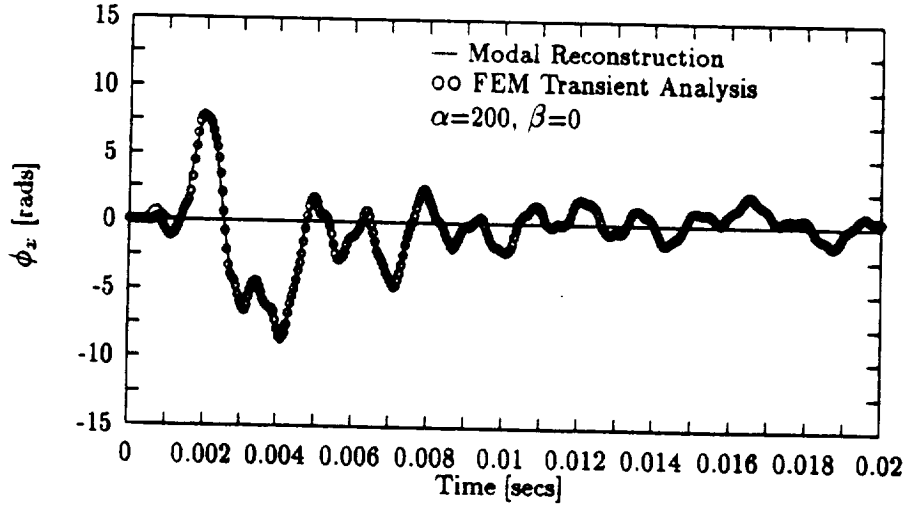

Figure 4.14: FEM transient and modal reconstruction ϕ_x comparison: $\alpha = 200$

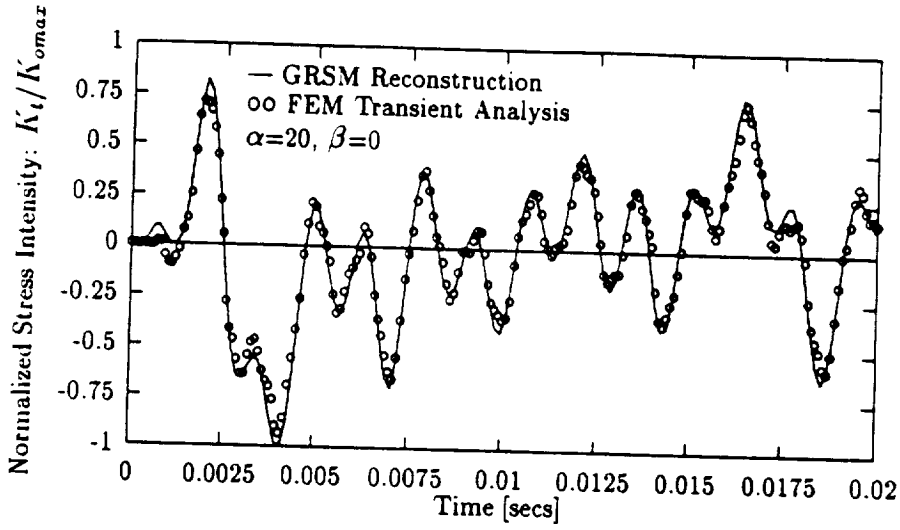

Figure 4.15: FEM transient and GRSM reconstruction K_t/K_{omax} comparison: $\alpha = 20$.

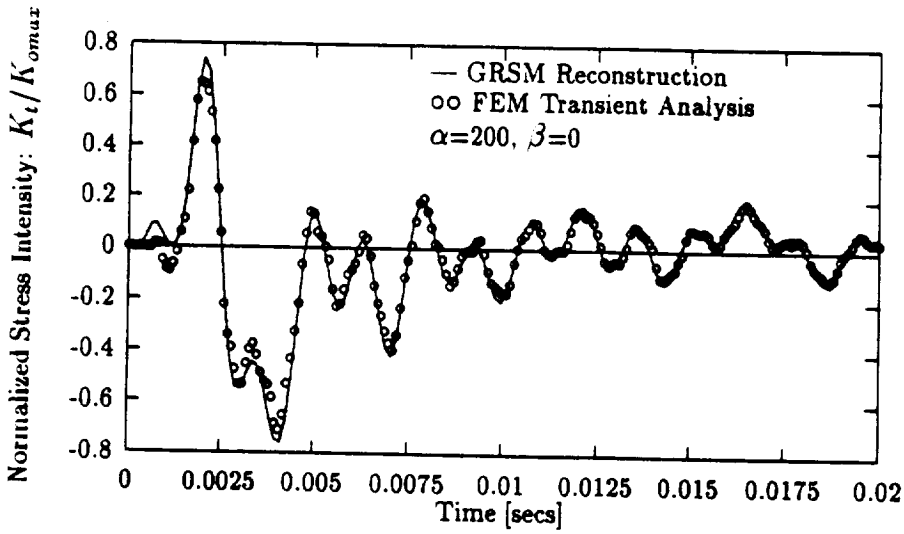

Figure 4.16: FEM transient and GRSM reconstruction K_t/K_{omax} comparison: $\alpha = 200$.

5. RANDOM LOADINGS

The effect of a random (or nondeterministic) loading of a panel is important because many real loadings that occur on aircraft or automobiles are of this type, and it can drastically affect the fatigue crack growth rate.

This type of loading usually has a high frequency content but a low stress level [14] and this makes it computationally expensive to analyze using time integration methods. In this section we explore two methods of analysis.

5.1 Random Loads

Our random forces used in the analyses were generated by using a random number generator. This utilized a multiplicative congruential random number generator with period 232 to return successive pseudo-random numbers in the range from 0 to 1. We require that there be an equal probability that the random number be negative as positive, therefore, 0.5 was subtracted at each time step. Such a sequence of numbers have a relatively broad and flat frequency spectrum. In our final step this random number sequence is multiplied by a force envelope. The first random force history and force envelope is shown in Figure 5.1.

The Fast Fourier Transform was used to transform the force from the time domain to the frequency domain and the result is shown in Figure 5.2. For this transform, a Δt of 100 μs along with 4096 transform points were used. In order to perform the convolution of $\hat{H}_k$ and $\hat{P}$, the frequencies of the two have to match. The frequency corresponding to the above transform parameters can be found by

$$\Delta f = \frac{1}{\Delta t N} \tag{5.1}$$

This gives a Δf of 2.4414 hertz or 15.34 rads/s. In performing force convolutions, it is required that the magnitude of the force spectrum be close to zero before the

Nyquist frequency is reached. It can be seen in Figure 5.2 that this is the case for this particular force history.

The modal frequency response values and $\hat{K}$ values using the GRSM method are used as the transfer functions and were convolved with the corresponding values of the force transform in the same manner as in Section 4. Once this convolution was formed, the inverse FFT was taken. The results from the inverse FFT were then compared to the baseline values from the transient finite element analysis.

5.2 Random Load Modal Analysis

The transient modal and finite element analysis are carried out in the same manner as discussed in Section 4. Figures 5.3 and 5.4 show the comparison between the modal and transient finite element results for the rotation response for a medium damping value of α=20, and a heavy damping value of α=200, respectively. The agreement is seen to be good between the two methods.

The corresponding comparisons for K_t between the transient finite element results from PlaDyn and modal results for are shown in Figures 5.5, and 5.6. These values of K_t were normalized similarly to Section 4 in that the maximum value of the moment history was multiplied by the static K value, and this was used as the normalizing factor. Again, the comparison shows good agreement for both methods.

As in the previous section, once the force ceases, the response very quickly settles into a damped single mode vibration.

The transient finite element analysis is computationally very expensive. Therefore, since a broad frequency spectrum is needed in order to account for the force amplitude, this method was not pursued further.

5.3 Random Load Spectral Analysis

In using the spectral method of convolving $\hat{P}$ with $\hat{H}_k$, the main obstacle is in determining a sufficient number of transform points. We showed in the previous section that a modal analysis is a convenient way of generating transfer functions. The results are obtained very quickly and a large frequency spectrum can be achieved along

with the desired increment of frequency. Being able to choose the frequency increment allows more freedom in choosing the number of transform points and the time increment.

Since the spectral analysis can be used to perform convolution of any frequency parameter, the frequency rotation response was used as $\hat{H}_u$, the transfer function, and was convolved with the force transform. The inverse FFT was then taken. As has been shown the rotation response gives a good indication of the trend of the stress intensity factor. The results for the comparison between the inverse FFT response and the baseline transient finite element results are shown in Figures 5.7 and 5.8. The comparison shows good agreement.

The modal frequency $\hat{K}$ values found by the GRSM method were used as the transfer function and were convolved with the transform of the force. The inverse FFT of the convolution was taken to get the time domain stress intensity factor values. The comparison between the stress intensity factor and the baseline transient finite element results are shown in Figures 5.9 and 5.10. As was expected based on the results from the response plots, the agreement was found to be good.

5.4 Long Duration Random Loading

As a final example, we consider a random loading of long duration. The force history used and its transform are shown in Figures 5.11 and 5.12, respectively.

Using this random force the transient modal analysis was performed. Since it has been established that the transient modal results give virtually equivalent results as the transient finite element, a comparison of the spectral modal results and the transient modal results will be made.

The analysis is carried out as before using transient modal analysis and modal convolution. Only one damping value was investigated for both of the methods used; that being a value for α of 20, and β of 0.

Using the responses obtained from the modal method and K_t values obtained by using the GRSM method as the transfer function and convolving each with the force transform, the spectral analysis is performed and compared to the modal transient

results. Figure 5.13 shows the comparison for the rotation response. Figure 5.15 shows the comparison of the transient K_t values. As was expected, the they are in good agreement.

A note should be made regarding the time increment chosen for the integration and the transform. It was found that the time increment used for taking the force transform had little effect on the results after the inverse FFT was taken and compared to previous results. On the other hand, the time increment chosen to generate the modal responses in order to do the post processing to gain the moment on the crack tip had a significant effect on the results. The time increment of $100\mu s$ in taking the force transform was used. An initial value of $50\mu s$ was used in the modal transient analysis. Upon comparing the ϕ_x and K_t values, it was seen that the agreement was not very good. Therefore, a finer time step was used for the modal transient integration and the comparison for these results are shown in Figures 5.14 and 5.16 on a reduced time scale for ease of comparison for the rotation and K_t results, respectively. These results show good agreement between the two methods.

5.5 Dynamic and Quasistatic K_t Comparison

The dynamic problem studied above will be put into perspective by considering the quasistatic problem. By quasistatic, we mean that for each discretized random load point the corresponding K_t value would be calculated by

$$K_t = K_o = \frac{6M_oP(t)\sqrt{\pi a}}{h^2} \tag{5.2}$$

where M_o is the constant applied moment, and P(t) is its scaling history time. For the random force the K_t values were calculated and normalized with respect to the K value found by using the maximum moment of 500 in the above equation for P(t). These results were then compared to the K_t values calculated for the modal transient analysis in the previous section. The comparison is shown in Figure 5.17. As can be expected the quasistatic K_t values follow the same pattern as exhibited by the random input. It can be seen that the values from the dynamic response and the quasistatic analysis are drastically different—as much as 400% on average. One of the reasons for the large difference is that for the dynamic analysis multiple resonances

are taken into account. This point can be illustrated by generating a histogram of the K_t values for these methods and comparing the results. Figure 5.17 was divided into increments along the y-axis of 0.5. At each time step, the magnitude of the response was checked to see in which increment it was contained. A summation of the number of responses for each increment was done and the results are shown in Figure 5.18. This figure indicates that if the quasistatic analysis method is used, only the lower amplitudes are taken into account; this is indicated by the high count number at the lower two increments. When the problem is analyzed using the modal transient method (or the GRSM convolution since they are comparable) the response will span more resonances and generate a greater spectrum of amplitudes. This is indicated in Figure 5.18 by noting that the count is significant for the higher increments indicating that the response is higher.

We now discuss how this history may influence damage growth. In the 1960's, Paris developed what is now known as the Paris equation [8] which is a curve fitting technique and is given by

$$\frac{da}{dN} = C(\Delta K)^m \tag{5.3}$$

where C and m are material constants and ΔK is the stress intensity range. The material constants, C and m may be found in reference books such as References [16] and [1]. Values for m range from 3 to 4 typically [8]. Both the quasistatic and dynamic histograms have the same total number of counts, they differ only in their amplitude spread. Because of the non-linearity in the damage model (the exponent m in the Paris law), we see that the few large amplitudes have a disproportionate effect on the damage.

Using this value of m in the above example would give a value of approximately 47 times the quasistatic value ($3^{3.5}$) or 70,500. This illustrates the importance of considering the dynamics of the problem.

5.6 Discussion

The problem of random loading on a structure can be very computationally intensive, therefore, performing analysis using a conventional finite element program such as

PlaDyn is usually not feasible. Modal analysis affords more flexibility in that the computational cost is in the eigenanalysis and once this is performed the cost for finding the time response is minimal for a given force history. The one drawback of the transient modal analysis is that it only gives the system response. In order to calculate the stress intensity factor, the moment on the crack tip is required. As pointed out in Section 4, the modal responses of the nodes around the crack tip are required and these responses dictate the moment exerted on the crack tip and are used in conjunction with a finite element package such as PlaDyn.

The method most convenient for analyzing many different force histories is spectral analysis. It was shown that using a spectral analysis along with a single modal frequency analysis gives results comparable to the transient finite element results. Therefore, many different random force histories can be analyzed using a combination of a single modal frequency analysis and spectral analysis, both of which have very low computational cost.

The combination of the spectral method and a forced frequency finite element analysis was not examined here since the computational cost of calculating an adequate number of transfer functions was prohibitive for the system under investigation. Using modal analysis in the frequency domain to get the transfer functions in combination with the spectral method was deemed the most useful because of its flexibility and relatively small computational cost. Another distinct advantage of the spectral method over the modal is that it is much more straight forward to execute even for a high frequency content, long duration loading. The drawback found in using the transient modal method is that the time increment must be small. For the spectral method the time window is dependent upon the number of transform points and the time increment of the transform; thus giving more flexibility for investigating the effects of a loading that may last a relatively long time.

The comparison between the quasistatic and the full dynamic response is important because the generated larger amplitudes can have a more significant effect on the damage.

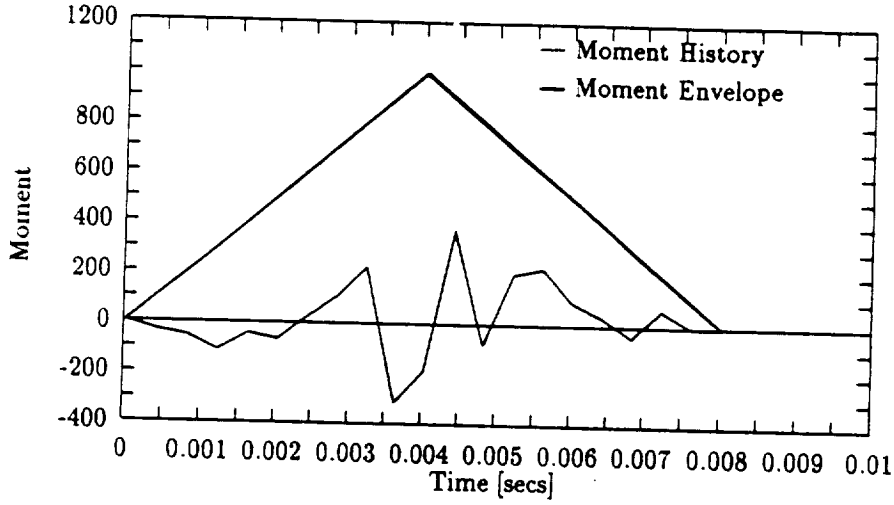

Figure 5.1: Random force history.

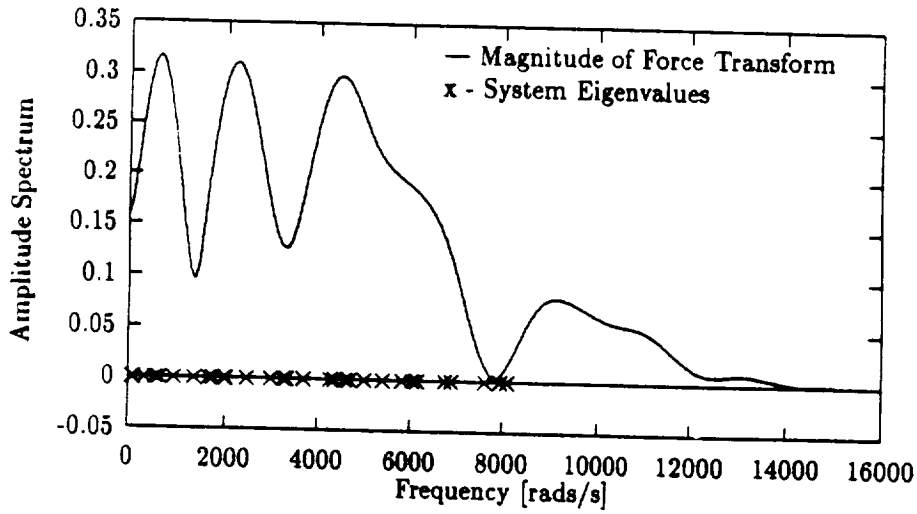

Figure 5.2: Amplitude spectrum of random force history.

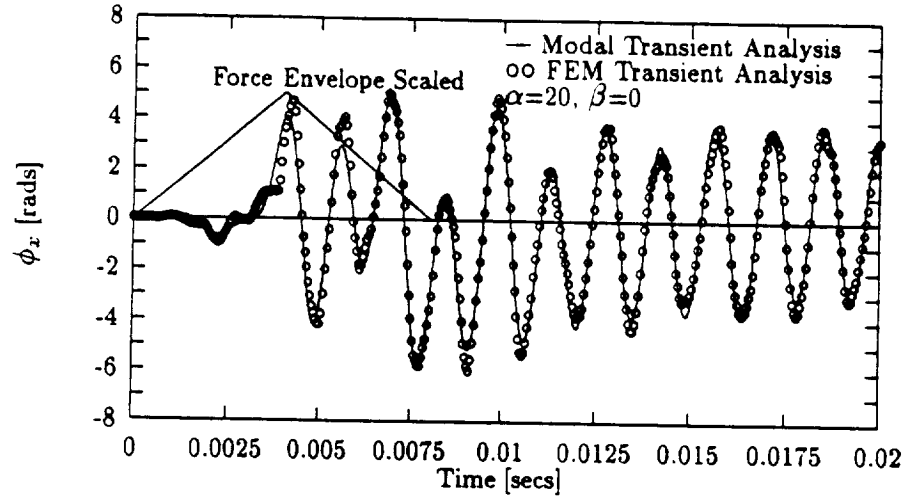

Figure 5.3: FEM and modal transient ϕ_x response comparison: $\alpha = 20$

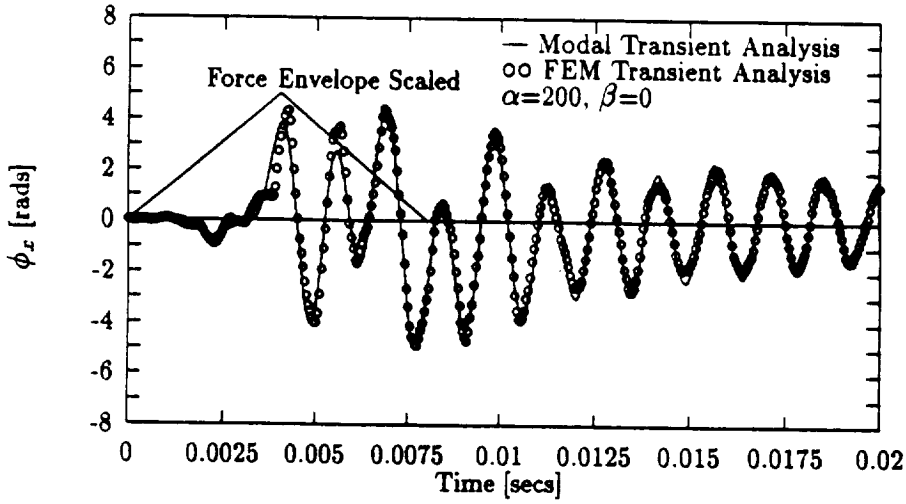

Figure 5.4: FEM and modal transient ϕ_x response comparison: $\alpha = 200$

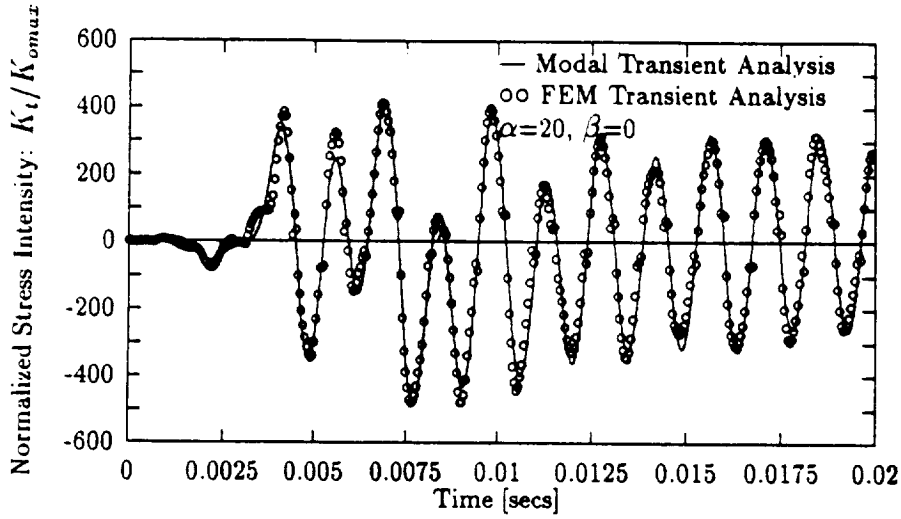

Figure 5.5: FEM and modal transient K_t/K_{omax} comparison: $\alpha = 20$.

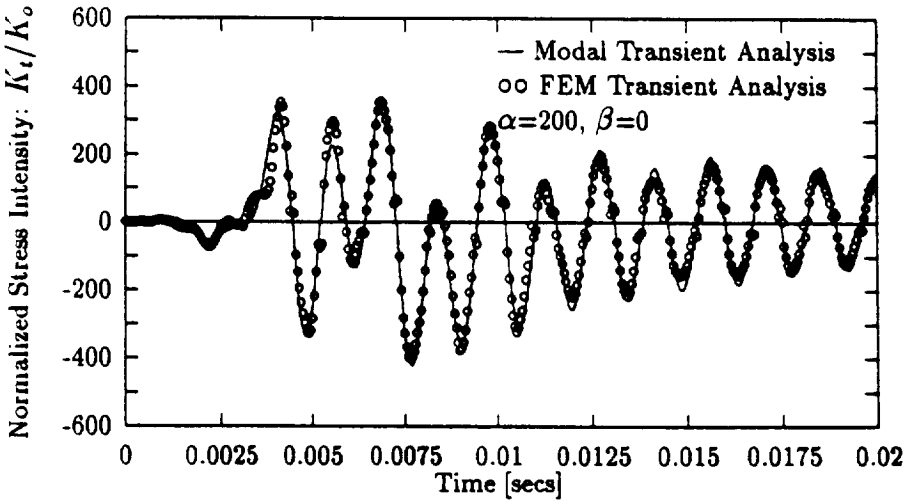

Figure 5.6: FEM and modal transient K_t/K_{omax} comparison: $\alpha = 200$.

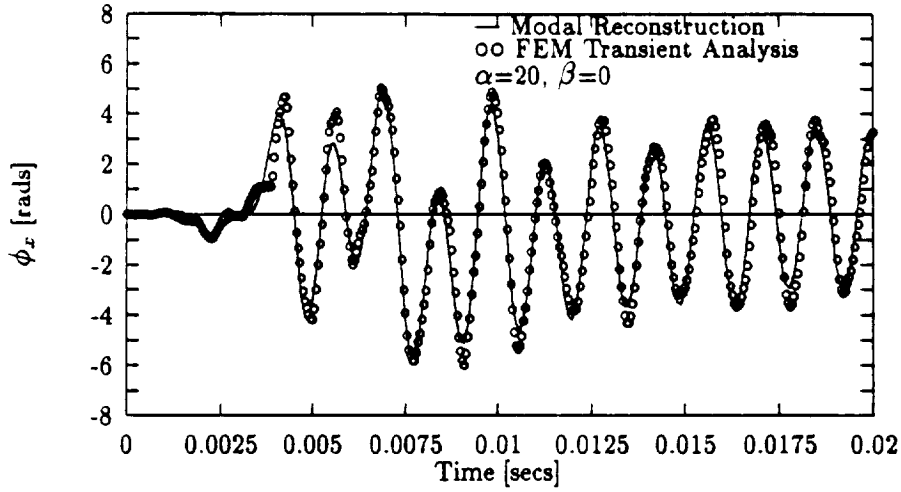

Figure 5.7: FEM transient and modal reconstruction ϕ_x comparison: $\alpha = 20$

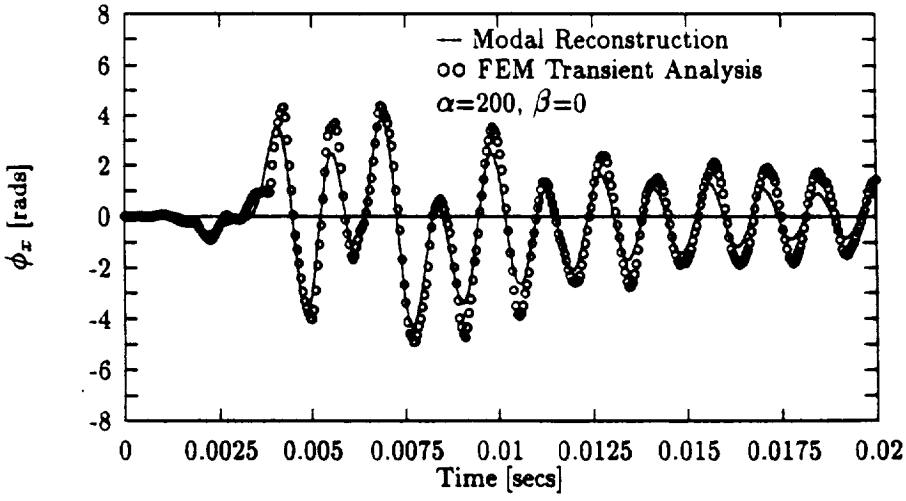

Figure 5.8: FEM transient and modal reconstruction ϕ_x comparison: $\alpha = 200$

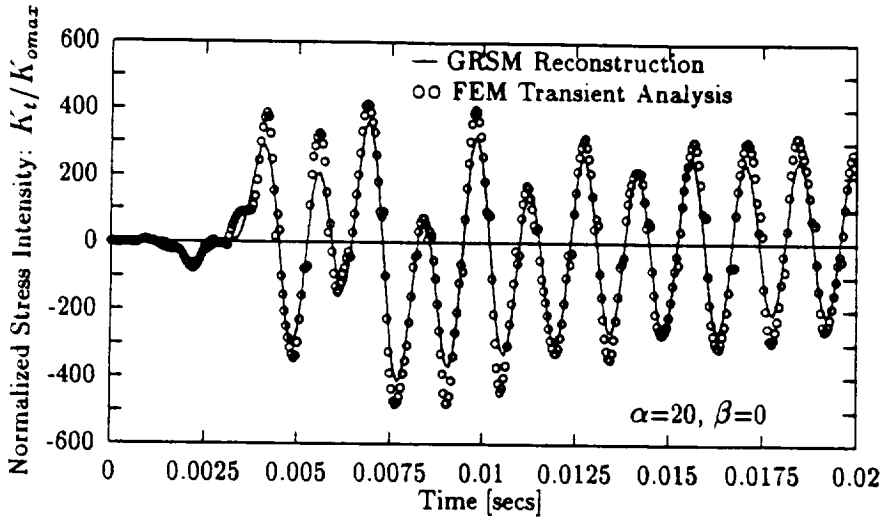

Figure 5.9: FEM transient and GRSM reconstruction K_t/K_{omax} comparison: $\alpha = 20$.

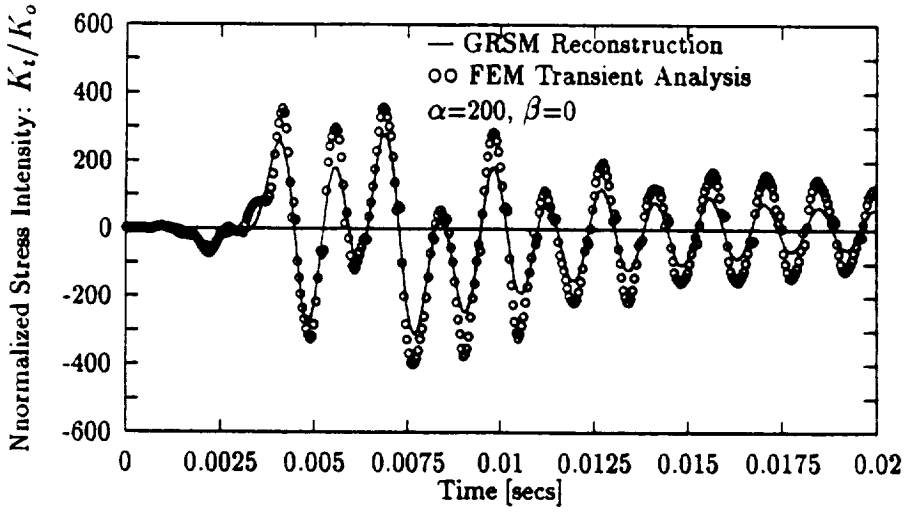

Figure 5.10: FEM transient and GRSM reconstruction K_t/K_{omax} comparison: $\alpha = 200$.

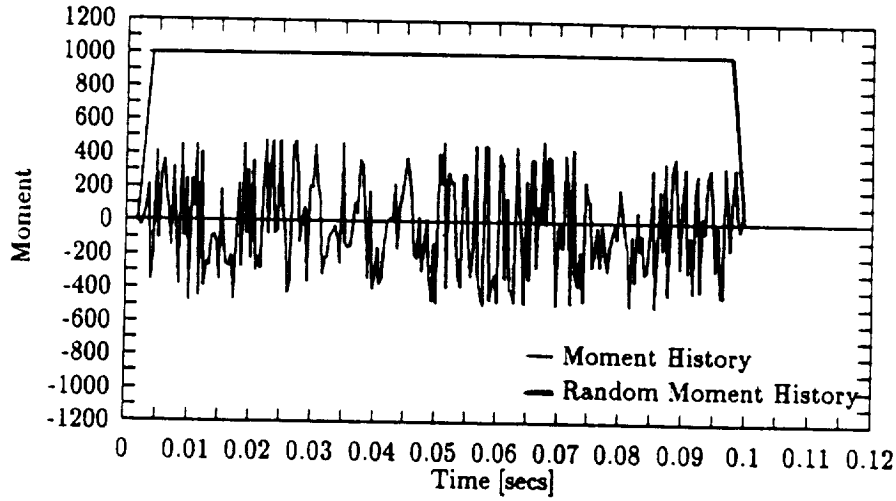

Figure 5.11: Long duration random force and force envelope.

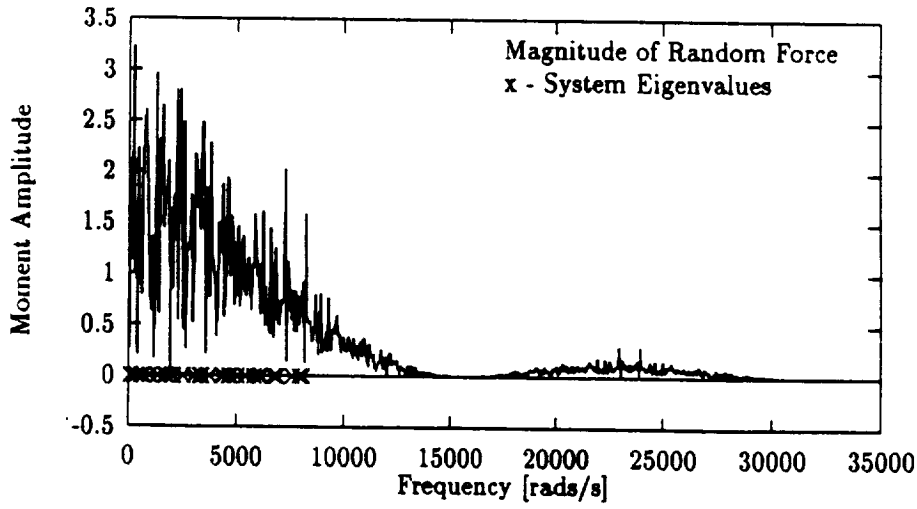

Figure 5.12: Amplitude spectrum of randon input.

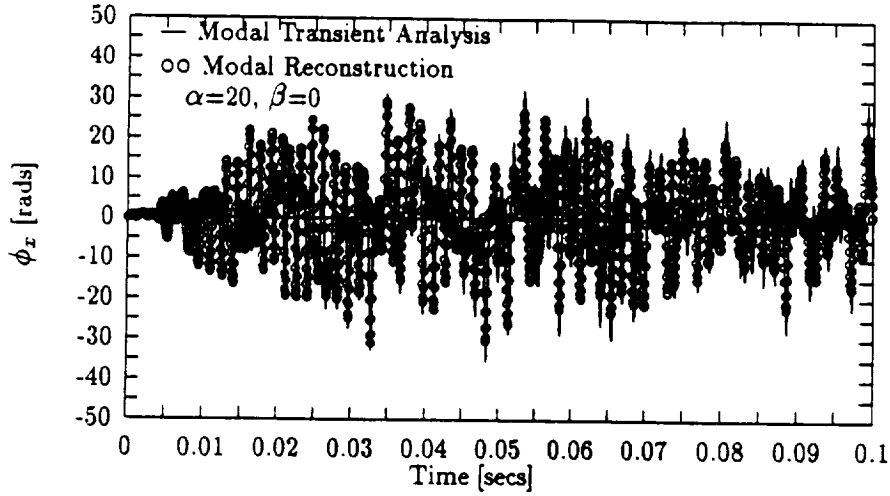

Figure 5.13: Modal and transient and modal reconstruction ϕ_x comparison: $\alpha = 20$

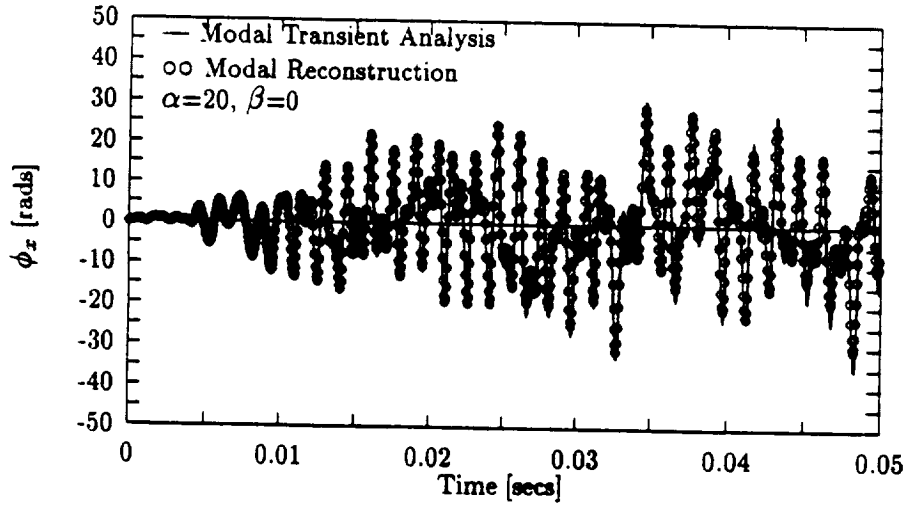

Figure 5.14: Modal transient and modal reconstruction ϕ_x comparison: expanded scale.

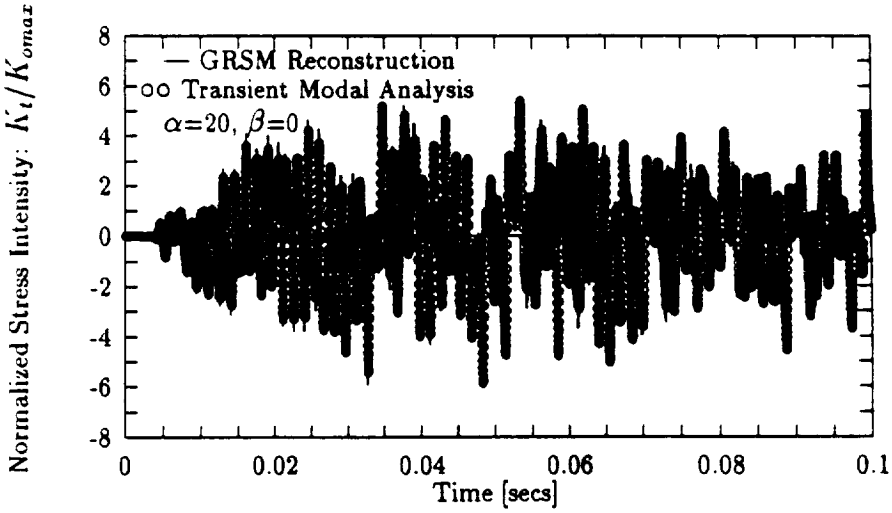

Figure 5.15: Modal transient and GRSM reconstruction K_t/K_{omax} comparison: $\alpha = 20$.

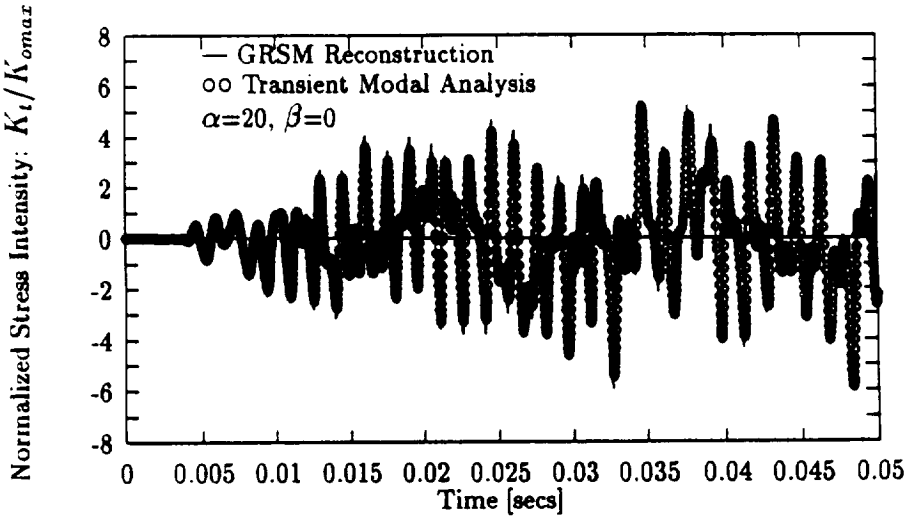

Figure 5.16: Modal transient and GRSM reconstruction K_t/K_{omax} comparison: expanded scale.

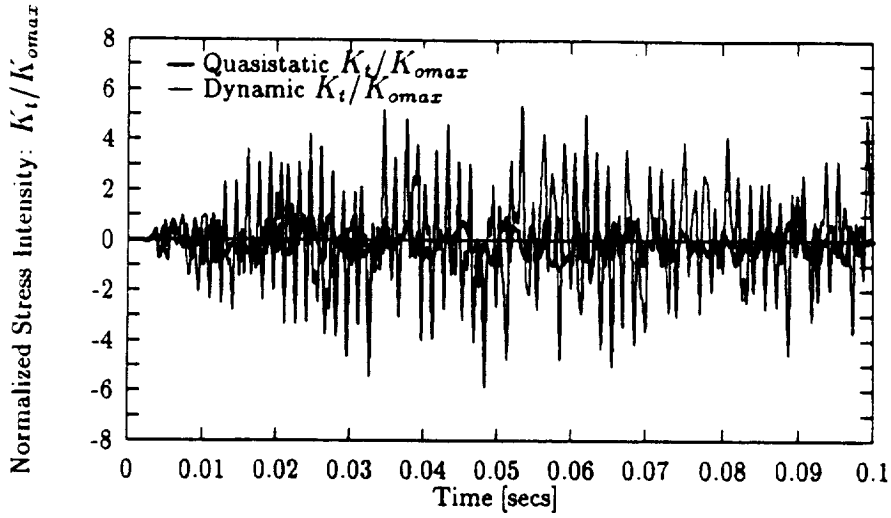

Figure 5.17: Quasistatic and modal dynamic K_t/K_{omax} comparison.

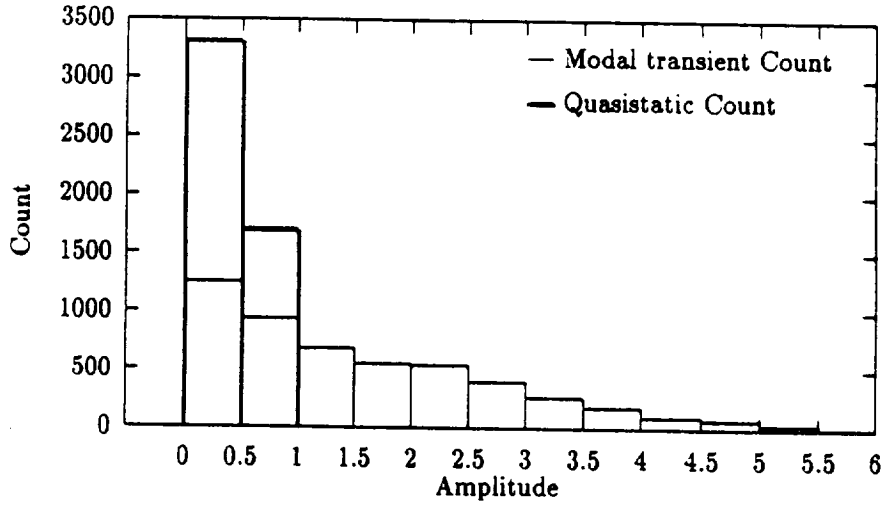

Figure 5.18: Histogram of quasistatic and dynamic K_t response.

CONCLUSIONS

The random dynamic loading of a panel with a crack is a very challenging problem both computationally and analytically. This report investigated some of the aspects of its challenge and effected a solution.

The finite element method plays a central role in the solution and we showed that the discrete Kirchhoff triangle element has very good properties for the solution of thin plate problems. While not specifically investigated here, its triangular shape allows generation of meshes to model arbitrary shaped regions such as holes, cutouts or curved cracks.

The virtual crack closure technique is a powerful method for K extraction but in its direct form for dynamic problems, it can be computationally expensive since a complete dynamic problem is solved for each loading. Also, it becomes less cost effective when long time responses are required as is the case for random loadings. The combination of this method with GRSM analysis seems to be a very powerful technique—the eigenanalysis is done once (for a limited number of modes) and then any type of loading can be applied. The frequency domain form of this also has significant advantages. In fact, the GRSM analysis makes it very convenient to alternate between a transient analysis and a forced frequency analysis.

Damping plays a significant role in the response of real structures— without it all structures would (theoretically) fail at resonance. We modeled multiple levels of damping and showed how it affects the dynamic response. In order to use modal analysis, however, it is necessary that the damping be proportional. From a practical standpoint, this is not a severe limitation since damping is usually not known very accurately. Consequently, proportional damping can be made an acceptable approximation.

For a random loading, it was shown that it is vital to consider the dynamics of the structure since multiple resonances may be spanned. Therefore, design should not be based on the quasistatic results since they significantly underestimate the actual response of the structure and hence the damage accumulation. This conclusion is based on the results found in using Paris' equation for calculating crack growth. A large difference between the quasistatic and the dynamic analysis was shown indicating that a dynamic analysis need be performed using one of the methods outlined here. The particular method used to perform the analysis would depend upon the problem specifications and requirements.

This research can now form the basis for the modeling of such difficult problems as the effect of random loading on the fatigue growth in structures.

References

[1] **Barsom, J.M.**, "Fatigue-Crack Propagation in Steels of Various Yield Strengths", *Trans. ASME, J. Eng. Ind.,*, vol. B73, No. 4, Nov 1971.

[2] **Batoz, J.L., Bathe, J.L., and Ho, L.W.**, "A Study of Three-Node Triangular Plate Bending Elements", *International Journal for Numerical Methods*, vol. 15 pp. 1745–1750, Jan 1980.

[3] **Cook, R.D.**, *Concepts and Applications of Finite Element Analysis*, John Wiley and Sons, New York., 1989.

[4] **Doyle, J.F.**, *Wave Propagation in Structures: An FFT-Based Spectral Analysis Methodology*, Kluwer Publishing, Boston, MA., 1989.

[5] **Doyle, J.F.**, *Static and Dynamic Analysis of Structures*, Kluwer Publishing, Boston, MA., 1991.

[6] **Dym, R. and Shames, R.**, *Energy and Finite Element Methods in Structural Mechanics*, Hemisphere, Washington., 1985.

[7] **Irwin, G.R.**, "Fracture", *Handbuch der Physic*, vol. 6 pp. 551, Jan 1958.

[8] **Kanninen, M.F. and Popelar, C.H.**, *Advanced Fracture Mechanics*, Oxford University Press, New York., 1985.

[9] **Kobayashi, A.S.**, *Experimental Techniques in Fracture Mechanics*, Iowa State University Press, Ames, Iowa., 1973.

[10] **Leissa, A.W.**, *Vibration of Plates*, Scientific and Techncial Information Division; Office of Tecnology and Utilization; National Aeronautics and Space Administration, Washington, D.C., 1969., 1969.

[11] **ModDyn**, *"Modal Analysis of Dynamic Systems"*, *ikayex* Software Tools, Lafayette, IN., 1992.

[12] **Petyt, M.**, *Introduction to Finite Element Vibration Analysis*, Oxford University Press, New York., 1990.

[13] **PlaDyn**, *"A Program for the Static and Dynamic Analysis of Folded Plates"*, *ikayex* Software Tools, Lafayette, IN., 1992.

[14] **Rizzi, S.A.**, "A Frequency Based Approach to Dynamic Stress Intensity Analysis", *American Institute of Aeronautics and Astronautics Journal*, pp. 2677–2683, 1991.

[15] **Rizzi, S.A., and Doyle, J.F.**, "Frequency Domain Stress Intensity Calibration of Damped Cracked Panels", *International Journal of Fracture*, vol. 7 pp. 180–181, Sep 1990.

[16] **Rolfe, S.T. and Barsom, J.M.**, *Fracture and Fatigue Control in Structures*, Prentice Hall, New Jersey., 1977.

[17] **Rook, D.P. and Cartwright, D.J.**, *Compendium of Stress Intensity Factors*, H.M.S.O., London., 1976.

[18] **Rybicki, E.R. and Kanninen, M.F.**, "A Finite Element Calculation of Stress Intensity Factors by a Modified Crack Closure Integral", *Engineering Fracture Mechanics*, vol. 9 pp. 931–938 1977.

[19] **Sih, G.C. and Paris, P.C. and Erdogan, F**, "Crack Tip, Stress-Intensity Factors for Plane Extension and Plate Bending Problems", *Journal of Applied Mechanics*, ASME 29, pp. 306–312 June 1962.

[20] **Stricklin, J.A., Haisler W., Tisdale, R., and Gunderson, R.**, "A Rapidly Converging Triangular Plate Element ", *American Institute of Aeronautics and Astronautics*, vol. 7 pp. 180–181, Sep 1968.

[21] **Timoshenko, S. and Woinowsky-Krieger, S.**, *Theory of Plates and Shells*, McGraw-Hill, New York., 1959.

[22] **Wu, W-F**, "Computer Simulation and Reliability Analysis of Fatigue Crack Propagation Under Random Loading", *Journal of Fracture Mechanics*, vol. 45 pp. 697–712, Aug 1993.

[23] **Young, M.J.** *Analysis of Cracked Plates Subjected to Out-Of-Plane Loadings.* PhD thesis, Purdue University, 1991.

QMS-PS 810

Version 47.2C

Defined Font Outlines

Times®-Roman
Times-Bold
Times-Italic
Times-BoldItalic

ITC Avant Garde®-Book
ITC Avant Garde-Demi
ITC Avant Garde-BookOblique
ITC Avant Garde-DemiOblique

Helvetica®-Narrow
Helvetica-Narrow-Bold
Helvetica-Narrow-Oblique
Helvetica-Narrow-BoldOblique

Helvetica®
Helvetica-Bold
Helvetica-Oblique
Helvetica-BoldOblique

Palatino®-Roman
Palatino-Bold
Palatino-Italic
Palatino-BoldItalic

ITC Zapf Chancery®-MediumItalic
ITC Zapf Dingbats®
Symbols Set

Courier
Courier-Bold
Courier-Oblique
Courier-BoldOblique

New Century Schoolbook-Roman
New Century Schoolbook-Bold
New Century Schoolbook-Italic
New Century Schoolbook-BoldItalic

ITC Bookman®-Light
ITC Bookman-Demi
ITC Bookman-LightItalic
ITC Bookman-DemiItalic

11926 pages printed

RAM size: 2.0 Mbytes

Interface: Centronics Parallel

QMS-PS 810